António Guevara Ferreira Exposto Rodriguez Lopez

Licenciado em Bioquímica

Phototermal therapy using gold nanoparticles

Dissertação para obtenção do Grau de Mestre em
Bioquímica para a Saúde

Orientador: Pedro Miguel Ribeiro Viana Baptista, Professor Doutor, FCT/UNL

Setembro, 2017

António Guevara Ferreira Exposto Rodriguez Lopez

Licenciado em Bioquímica

Phototermal therapy using gold nanoparticles

Dissertação para obtenção do Grau de Mestre em
Bioquímica para a Saúde

Orientador: Pedro Miguel Ribeiro Viana Baptista, Professor Doutor, FCT/UNL

Júri:
Presidente: Prof.ª Doutora Maria Teresa Nunes Mangas Catarino
Arguente: Prof. Doutor João Carlos dos Santos Silva e Pereira de Lima
Vogal: Prof. Doutor Pedro Miguel Ribeiro Viana Baptista

Faculdade de Ciências e Tecnologias, Universidade Nova de Lisboa

Setembro, 2017

Phototermal therapy using gold nanoparticles

ACKNOLOWDGEMENTS

Ludwig Wittgenstein once said that knowledge is in the end, based on acknowledgment, and he was not far from the truth. This all year was an indescribable journey, a kind of roller-coaster, full of ups and downs, a series of incidents that lead me to the opposite extremes of horror and ecstasy.

I hereby want to express my gratitude to you all, all the people that contributed to this work, without them this thesis would not come to the light of day, or even started. I am afraid that words could not be enough to express my thankfulness, but here it goes. I would like to especially thank to:

Professor Pedro Viana Baptista, my supervisor, for all the opportunities he gave me throughout the year; for all the guidance, the time, the mighty advices; for all the help he gave me in my scientific and academic growth; and most of all for trusting in me. I am sincerely thankful.

Professor João Sottomayor for all the assistance with the densitometer and pycnometer, as well as the willingness to receive me in his office and answer all my questions.

Professor João Carlos Lima to arrange 5 minutes to talk to me, even when ill, and pointing me the right direction when I was not entirely sure of what to do to reach my goal.

Professor Madalena Dionisio for the precious help as well as the availability for answering any doubts that came out throughout the experiments with the Differential Scanning Calorimetry.

Professor Alexandra Fernandes, Professor Jaime Mota, Professor Carlos Salgueiro and Professor Mario Diniz for the kindness, and all the support and advices along this year.

Professor Manolis Matzapetakis and Professor Antonio Baptista for not allowing me to lose hope in my ideas, and Professor Ricardo Louro to be an inspiration. I always remember one of your most iconic phrases:" NMR can save almost all the problems in the World"

Pedro Pedrosa and Rita Mendes, for guiding me during my first month on the lab and to

be always available to help me when I was in need of help.

All the members of lab 315 and 319, the one's that inspired and motivated to go there (Fábio Carlos and Bruno Veigas); the one's there were there and gave me all the support they could: Milton Cordeiro, Fabiana Paradinha, Raquel Vinhas, Ana Sofia, Catarina Rodrigues, Luis Raposo, Vanessa Silva, Andreia Carvalho, Ana Silva, Letícia Fialho, Cinthia Barroco, Catarina Brás, Rita Gomes, Miguel Padilha, Mariana Cunha, Rita Fernandes; the one's that left and finally the one's that our paths crossed each other even for a brief moment in time, Suzilaine and Inês Martins, I did not forget you. A special thanks to Cindy Oliveira, Beatriz Coelho and Filipa Correia, you were my light, my guiding star, sometimes with just a smile (you give so many, in a few seconds…). I have not got enough words in my vocabulary for you, you are so damn special!

The Photochemistry group (Verónica Simões, Andreia Forte, André Seco, Ana Lúcia, Marcos) for making me feel like I was at home when I spent all afternoons at the DLS.

My friends (spread across the globe), for always being there, for the advice and endless support and motivation that gave me, not only throughout the year but through life. I could name persons but they are too many and I do not want to particularize, all of you were and are special in my mind and in my heart.

My family for all the faith, the love, the strength and support, for being my rock. Especially for my parents that put up with me in my darker and annoying moments.

My colleagues, for all the things they taught me.

To Daniela, for entering my life when I did not know I needed you.

You all are the epitome that in life if you do your path alone, you go faster, but if you go together, you go further. My path was long, hard, but I never gave up, thanks to you all.

António Lopez

“A life without challenges is not worth living.”
Socrates

“You can know the name of a bird in all the languages of the world, but when you're finished, you'll know absolutely nothing whatever about the bird... So let's look at the bird and see what it's doing -- that's what counts. I learned very early the difference between knowing the name of something and knowing something.”
Richard P. Feynman

“We did not ask for this room or this music. We were invited in. Therefore, because the dark surrounds us, let us turn our faces to the light. Let us endure hardship to be grateful for plenty. We have been given pain to be astounded by joy. We have been given life to deny death. We did not ask for this room or this music. But because we are here, let us dance.”
Stephen King

Para a Margarida Alice –
Que a Primavera sempre perdure

RESUMO

O cancro é uma das principais causas de morte em todo o mundo. Tal mortalidade deve-se, maioritariamente, não à patologia em si, mas aos efeitos colaterais dos tratamentos existentes como a quimioterapia e a radioterapia. De forma a ultrapassar os problemas de falta de seletividade e especificidade das terapias existentes, novas alternativas encontram-se atualmente em investigação.

A terapia fototérmica usa a luz para induzir calor localmente, levando à morte celular. As células cancerígenas são mais vulneráveis ao aumento de temperatura devido ao fraco fornecimento de sangue e à falta de dissipação de calor. Geralmente, esta terapia emprega radiação infravermelha próxima permitindo uma penetração profunda nos tecidos e evitando a sua absorção por parte de certas biomoléculas como a hemoglobina. Comparando com as terapias convencionais, a terapia fototérmica revela vantagens únicas na terapia do cancro, incluindo alta seletividade e especificidade e mínima invasividade.

As nanopartículas de ouro possuem propriedades óticas, eletrónicas e térmicas únicas para a terapia fototérmica. Além disso, estas são fáceis de sintetizar em meio aquoso e podem ser facilmente funcionalizadas com uma ampla gama de biomoléculas. Modulando os parâmetros geométricos e físicos destas nanoestruturas, como a forma e o tamanho, os picos de ressonância plasmónica das nanopartículas de ouro podem ser sintonizados para a região do infravermelho próximo ou na região visível. Ao usar radiação de luz com uma frequência que se sobrepõe fortemente à banda de absorção do plasmão das nanopartículas, pretende-se que o procedimento de conversão fototérmica possa ser altamente eficiente.

O objetivo deste trabalho prende-se com a caracterização fototérmica de nanopartículas de ouro com diferentes tamanhos com o intuito de utilização futura na ablação fototérmica de células cancerígenas. A síntese e a funcionalização de nanopartículas de ouro com diferentes tamanhos foram realizadas com sucesso. Usando os ensaios de calorimetria, concluiu-se que as nanopartículas de ouro com um revestimento de PEG têm uma capacidade de conversão fototérmica maior do que aquelas com cobertura de citrato e que as nanopartículas de ouro menores são mais eficientes a converter luz em calor do que as maiores.

Palavras-chave: Cancro; Nanotecnologia; Terapia fototérmica; Nanopartículas de ouro.

ABSTRACT

Cancer is one of the leading causes of mortality worldwide. The fact that most people do not actually die from the cancer itself, but from the side effects of the conventional treatments (e.g. chemotherapy and radiation) has led scientists to find new therapies that can surpass the problem with lack of selectivity and specificity.

Nanotechnology is still a field in development but it could overcome these problems. It offers great potential in the biomedical field, in imaging, diagnostics, and therapy.

Photothermal therapy uses light to induce heat that leads to cell death. Cancer cells have proven to be more vulnerable to increase of heat due to poor blood supply and lack of heat dissipation. Generally this therapy employs near infrared radiation, which allows deep tissue penetration, thus allowing the evasion of absorbance of biomolecules (e.g. hemoglobin). Comparing conventional therapeutic modalities, photothermal therapy shows unique advantages in cancer therapy including high selectivity and specificity, and minimal invasiveness.

Gold nanoparticles possess unique optical, electronic and thermal properties for photothermal therapy. Moreover, they are easy to synthetize in aqueous media and can be easily functionalized with a wide range of biomolecules. Modulating the geometric and physical parameters of nanostructures such as shape and size, the plasmon resonance peaks of gold nanoparticles could be tuned to the near-infrared region or the visible region. By using light radiation with a frequency that strongly overlaps the nanoparticle plasmon absorption band, the aim is that the photothermal conversion procedure could be highly efficient.

The purpose of this work was to perform a photothermal characterization of gold nanoparticles with different sizes with the perspective of downstream application to photothermal ablation of cancer cells. Synthesis and functionalization of gold nanoparticles with different sizes were performed successfully. Using calorimetry it was concluded that “PEGylated” gold nanoparticles have higher photothermal conversion capacities than the ones with a citrate capping, and that smaller gold nanoparticles are more efficient in converting light to heat than the bigger ones.

Keywords: Cancer; Nanotechnology; Photothermal therapy: Gold nanoparticles.

TABLE OF CONTENTS

FIGURE INDEX

TABLE INDEX

EQUATIONS INDEX

ACRONYMS AND LIST OF ABBREVIATIONS

Abs	Absorbance
AuNPs	Gold Nanoparticles
AuNPs@Citrate	Gold Nanoparticles with citrate capping
AuNPs@PEG	Gold Nanoparticles with PEG capping
CW	Continuous Wave mode
DSC	Differential Scanning Calorimetry
DLS	Dynamic Light Scattering
DMEM	Dulbecco's Modified Eagle Medium
DTNB	5,5'-dithio-bis(2-nitrobenzoic) acid
GLP	Good Laboratory Practices
HD	Hydrodynamic Diameter
LDI	Laser Diode Intensity
LSPR	Localized Surface Plasmon Resonance
NIR	Near Infra-Red
PEG	Polyethylene glycol
PI	Polydispersity Index
PTT	Photothermal Therapy
Pul	Pulsed mode
ROS	Reactive Oxygen Species
RT	Room Temperature
SD	Standard Deviation
SDS	Sodium Dodecyl Sulfate
SPR	Surface Plasmon Resonance
TEM	Transmission Electron Microscopy
UV-Vis	Ultraviolet-Visible

List of symbols

C	Concentration
Cp	Specific heat
Δ (delta)	A change in a variable
E	Energy
η (eta)	Yield

I0		Initial light intensity
I		Light intensity after it passes through the sample
l		Optical path
ρ	**(rho)**	Density
Q		Heat transfer

1. INTRODUCTION

1.1. Cancer: An overview

Since the birth of Mankind, disease has been a common denominator throughout all generations. The arise of new and worse illnesses has led Mankind to seek a way to cure all misfortunes that affect all his similar in order to restore hope and "stability" to our lives.

Diagnosis and treatment are two crucial factors in keeping people healthy. To attain this, it is paramount to make a diagnosis as early as possible and perform a highly selective and specific treatment, with no side effects.

According to the World Health Organization (WHO) recent reports, cancer is the second leading cause of mortality worldwide, with 8.8 million deaths only in 2015 (in **Figure** 1 is possible to see cancer incidence around the World from 2005-2015). Almost 1 in 6 deaths is due to cancer. In the past year (2016), 1,685,210 new cancer cases and 595,690 cancer deaths were estimated to occur in the United States. And the issue is far-off from being solved. The global cancer rates could increase by 50% by 2020, and it is expected to rise by about 70% over the next 2 decades [1-3].

Although remarkable progress has been made in the last 50 years, we are not close to understanding the molecular mechanisms of this disease, as well as the search for new approaches of treatment that rely on selectivity and specificity concerning cancer cells. [2,3] This is where nanotechnology enters. It offers a great diversity of tools that can be very helpful for cancer diagnostics and therapy [2, 3].

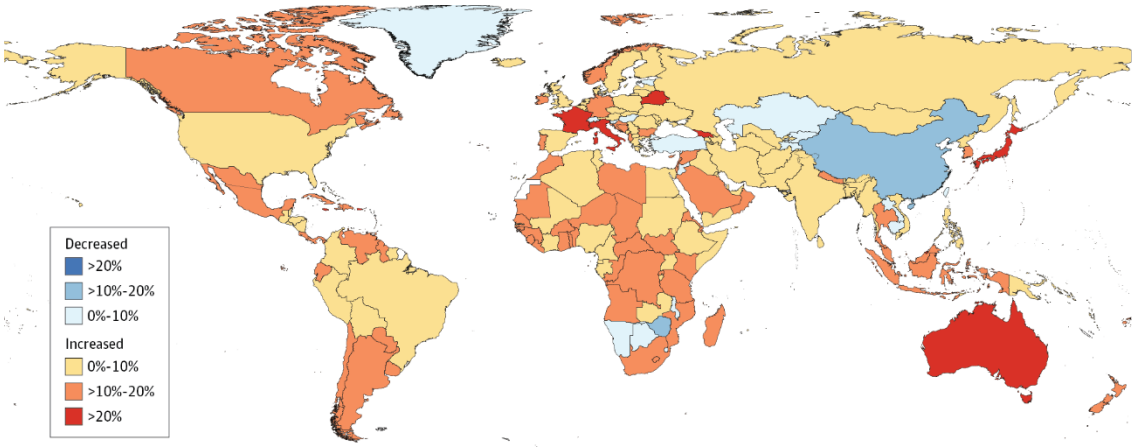

Figure 1: Relative changes in age-standardized cancer incidence rates in both sexes for all cancers in 195 countries or territories from 2005 to 2015 [4].

1.2. Nanotechnology

The concept of nanotechnology was first (indirectly) raised by Richard Feynman in a talk entitled "There's plenty of room at the bottom" in an American Physical Society meeting at Caltech in 1959 (**Figure 2**) [5,6]. Nowadays, it can be defined as the study and manipulation of materials with dimensions between 1 and 100 nanometers [7]. Nanomaterials have been used, even though inadvertently, since ancient times. A great example is the use of gold nanoparticles (AuNPs) in medieval cathedrals' stained glass windows (**Figure 3**) [3, 8-9].

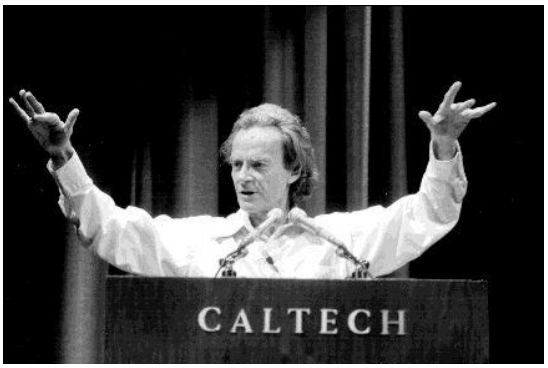

Figure 2: Richard Feynman on Caltech giving his lecture "There's plenty room at the bottom". http://www.kurzweilai.net/there-s-plenty-of-room-at-the-bottom (1/07/2017).

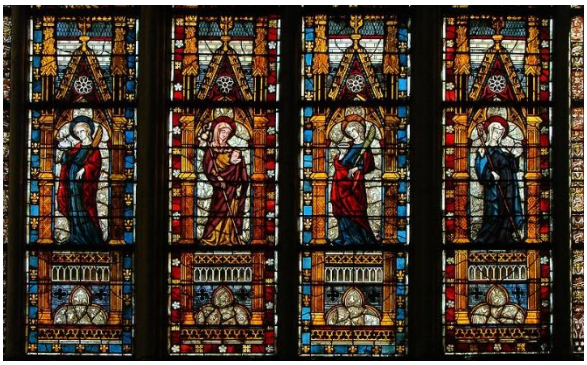

Figure 3: Stained glass containing gold nanoparticles in Troyes cathedral in France. https://cecilebester.wordpress.com/2013/06/18/the-beauty-of-nanoparticles/ (1/07/2017).

It was just in the last decade that the interest on these materials has emerged, due to their outstanding electrical, optical, and chemical properties, high stability and biological compatibility, controllable morphology and size dispersion, easy surface functionalization, as well the wide-range of applications they present [10-11]. The feature that makes nanomaterials stand out from their bulk materials is the high surface-area-to-volume ratio, which makes them a tool that offers great potential in the biomedical field, in imaging, diagnostics, and therapy [12, 13]. The most common bioapplications that have been used so far are labeling, delivering, heating, sensing, and detection, using several approaches, such as gene delivery, tumor targeting, or drug delivery, especially in cancer therapeutic [14, 15]. Examples of these nanomaterials are: carbon nanotubes, quantum dots, dendrimers and noble metal nanoparticles [16]. This thesis will focus on the applications of the later.

1.3. Gold Nanoparticles

AuNPs have been extensively studied and applied in several concepts of nanotheranostics (the use of nanotechnology for the diagnostic and therapy of different diseases), due to their unique optical, electronic, thermal and physical properties [17]. In the following subsections, it will be outlined some important aspects about these nanomaterials, like the synthesis, functionalization, properties and applications. This is important to perceive the importance of this work, due to the fact that gold nanoparticles are the core of what will be done next.

1.3.1. Synthesis and functionalization

In 1857, Faraday synthesized colloidal gold nanoparticles for the first time by reducing gold chloride with phosphors [6]. Almost 100 years after, Turkevich et al. simplified the method by using sodium citrate as reducing agent [18]. Since then, a wide variety of papers have been published about the subject. These mentioned different reduction agents, diverse capping agents, different sizes, different shapes, resulting in the end in solutions with different stabilities, and with higher or lower monodispersivity [19, 20]. Here are a few examples of the different procedures of AuNPs' synthesis: Schmid method, Brust–Schiffrin method and seed mediated growth method [21]. The size and shape of AuNPs is determined mainly by salt concentration, temperature, nature of capping agents, and rate of addition of reactants [22, 23].

Gold nanoparticles can be easily functionalized with a wide range of (bio) molecules (**Figure 4**). In order to do that, several methods have been devised. In spite of the fact that each technique has its specific purposes (due to its unique characteristics), the main goal is to increase the stability and affinity of AuNPs to biological molecules, as well as to use them as drug carriers into the cells with increased specificity. Gold nanoparticles are usually functionalized with one or a combination of biomolecules such as polyethylene glycol (PEG), peptides, tumoral markers, polymers, drugs, fluorescent dyes, oligonucleotides (i.e. siRNA, ssDNA), antibodies. All of them are easily attached to the nanoparticle surface [11, 24-25].

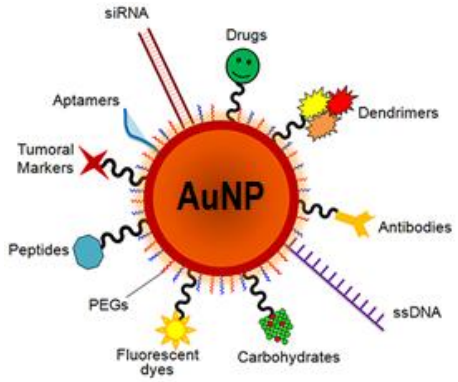

Figure 4: Different moieties that could be attached to the surface of a gold nanoparticle. Adapted from [11].

In Nanomedicine, the ability to easily render a biological function to inorganic nanostructures is of utmost importance [26]. Using citrate stabilized gold nanoparticles can make that possible. Since citrate interactions with gold are weak (adsorption), functionalization with biomolecules is generally easy through amine and thiol groups that interact strongly with gold (chemisorption) [27].

Giersig and Mulvaney first described the first robust gold nanoparticles by stabilizing them with thiolates using the strong bond between the soft gold acid and the soft thiolate base. Due to the fact that thiol groups bind to gold surfaces with high affinity, most frequently thiol modified ligands are used as stabilizing agents which bind to the surface of the AuNPs by formation of gold-sulfur bonds [28].

In this work, PEG (with a thiol end) was used to functionalize the AuNPs. "PEGylation" of nanoparticles is one of the most used methods. This hydrophilic and flexible polymer increases the stability and half-life of the gold nanoparticles (thus obtaining long circulating nanoparticles), and provides a very good biocompability with the human body. PEG creates a "hydration shell" surrounding the nanoparticle, preventing therefore opsonin-nanoparticle interaction (**Figure 5**), which is the first step of the recognition by the immune system. As for toxicity, it is diminished only in certain sizes [29, 30].

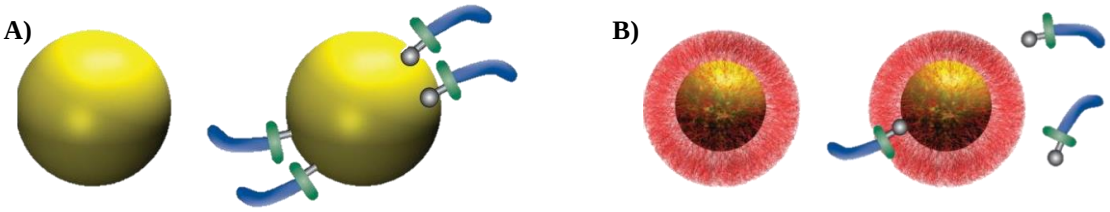

Figure 5: A) The effect of opsonins in bared gold nanoparticles B) The effect of opsonins in "PEGylated" gold nanoparticles [30].

1.3.2. Properties of gold nanoparticles

The most remarkable physical property of AuNPs is their size, which affects their surface-area-to-volume ratio and colloidal stability in solution [8]. It was Faraday that first stated that gold nanoparticles possess a reddish color due to its size. Since that moment, the interaction between light and AuNPs has been a target of interest [31].

When matter interacts with light, several phenomena occur. Light can be absorbed, scattered (i.e. Raman or Rayleigh scattering) or absorbed and re-emitted (i.e., fluorescence). In the presence of gold nanoparticles all these phenomena are strongly enhanced due to the unique interaction of light with the free electrons on their surface. Since light wavelength and nanoparticles are at the same scale, when gold nanoparticles are exposed to it, its electromagnetic field causes a collective and coherent oscillation of the conduction-band electrons at the surface of the nanoparticles, forming instantaneous dipoles. This phenomenon is called Surface Plasmon Resonance (SPR) [**Figure 6**] [8, 32].

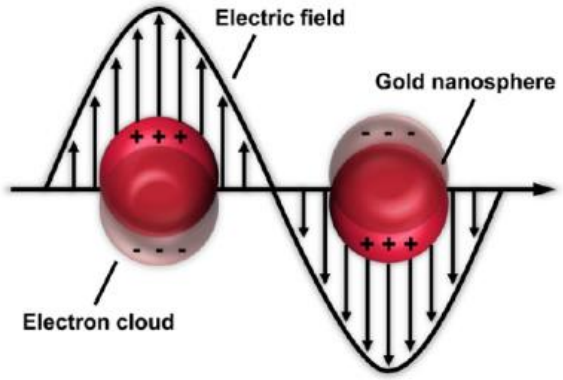

Figure 6: Schematic of the localized surface plasmon resonance on gold nanospheres. Upon illumination at resonant wavelengths, the conduction band electrons of the gold nanoparticles' surface are delocalized and undergo collective oscillation [33].

The SPR frequency is dependent on the type of the metal, the size and shape of the metal nanoparticles, the dielectric constant of the surrounding medium. This dependence enables the possibility of tuning the optical properties of these nanostructures. When the size increases, the SPR maximum slightly redshifts. This red-shift also occurs when the nanoparticles form assemblies or aggregates, but in these case it is to the Near Infra-red (NIR) region. Changing the shape from a sphere to a rod, the absorption spectrum splits into two bands: a stronger long-wavelength band in the NIR region due to the longitudinal oscillation of electrons and a weaker short-wavelength band in the visible region around [34, 35]. The present work is focusing in spherical particles.

Furthermore, the addition of salt and changes in pH leads to an increase of instability of the colloid, due to fact that there is a change in the dielectric constant of the media, momentary dipoles are generated at the nanoparticles' surface, reducing the repulsion between them and promoting their irreversible aggregation. Aggregated nanoparticles behave as bigger nanoparticles despite the fact that they are not chemically bonded. The solution acquires a blueish appearance. This occurs because when AuNPs are close enough, they change their optical properties, behaving as single bigger particles and shifting the SPR band to longer wavelengths. This ability to change color when aggregation happens is quite remarkable, and it is has been used extensively in diagnostic tests [32, 36-38].

1.3.3. Applications

Currently the most successful cancer treatment method usually involves invasive processes including chemotherapy, radiation, surgery or a combination of these.

Surgery has the purpose of physically remove the tumor, howbeit this is not always feasible [21, 39]. As for chemotherapeutic drugs, they have significant side effects due to its toxicity to normal cells. Another important fact is that cancer cells can develop resistance to these drugs. As for radiotherapy, the use of high energy ionization particles (X-rays, gamma rays or electrons) to damage cell and tissue at a molecular level to eradicate remaining cancer cells, it can cause damage to the healthy tissues close to the cancer cells, in the path of the radiation beam or in the surroundings (bystander effect) [21, 39-40].

Tremendous efforts have been devised by scientists and physicians to enhance these traditional treatments. Howbeit, selective methods are still required which can harm cancer cells hardly without destroying the healthy tissue [40].

Over the last decade researches have made many efforts to use AuNPs for cancer treatment. It is demonstrated that gold nanoparticles have an immense potential to enhance its efficiency [41].

As to the currently available gold nanoparticle-based therapeutic approaches (**Figure 7**), they can be classified into four main types [41]:

(1) **Photothermal therapy (PTT)**: minimally invasive treatment method in which photon energy is converted to thermal energy in order to induce cell death [41].

(2) **Photodynamic therapy:** consists in the selective destruction of targeted cells by a combination of light and light sensitive drug known as photosensitizers [41].

(3) **Radiotherapy**: consists in enhancing the radiosensitivity of cancer cells using kilovoltage or megavoltage energies [41].

(4) **Drug delivery**: AuNPs act as vectors for delivery of molecular cargo into a target [41].

This thesis is focused on the study and characterization of the potential of gold nanoparticles to do photothermia with the perspective of doing photothermal therapy.

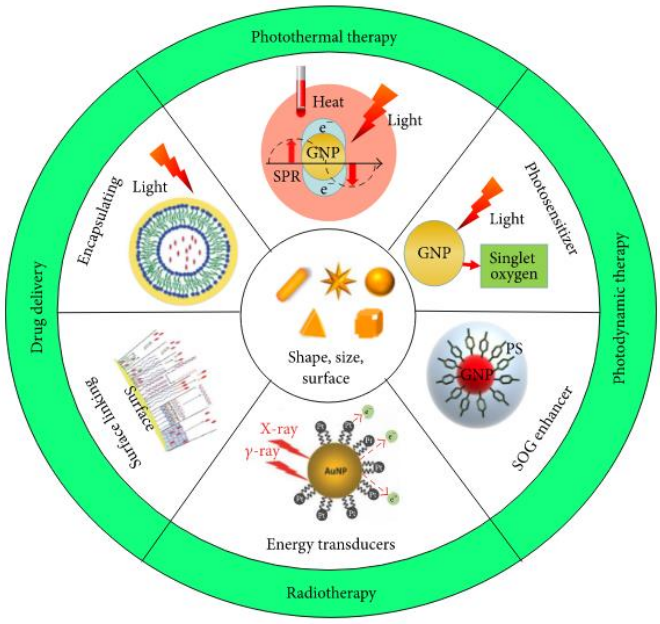

Figure 7: Current gold nanoparticle-based therapeutic approaches [41].

1.4 Photothermal therapy

The use of heat to treat illnesses has been a habit for ages. According to History, in 1700 B.C., a glowing tip of a firedrill was used to treat breast cancer. Thermal therapy has proven to be a good alternative to conventional oncological approaches. Heating sources including near infrared, visible light, radiofrequency waves, microwaves, and

ultrasound waves have been used to induce moderate temperature rise in a specific target region to destroy the cancer cells, clinically termed as hyperthermia. However, they all present a problem of destroying the tumors selectively. For a successful thermal therapy, hyperthermia should be confined to the target tumors without harming surrounding healthy tissues [21, 31].

Neoplastic cells were shown to be more vulnerable to temperature elevation than normal tissue cells. Studies have shown that laser power threshold required to kill the cancerous cells was less than half of that required to kill noncancerous cells. This happens because of their reduced heat tolerance compared to normal tissue, which is due to their poor blood supply. Moreover, the heat dissipation through blood flow in tumors is less effective than in normal tissue, which may contribute to a higher rise in temperature in tumor cells than in normal ones [21, 31].

Administration of AuNPs in cancer tissues followed by laser irradiation can offer the advantage of less-invasive and effective modality over the conventional treatment methods, as it combines a minimal systemic toxicity, rapid and effectiveness of heat deposition with a highly selective destruction of tumor cells [21, 31].

The photothermal properties of gold nanoparticles have been studied by Link and El-Sayed, who have shown that the photoexcitation of metal nanostructures results in the formation of a heated electron gas that subsequently cools rapidly (in approximately 1 picosecond) by exchanging energy with the nanoparticle matrix. This is succeeded by phonon–phonon interactions where the nanoparticle lattice cools down quickly by exchanging energy with the surrounding medium. This rapid energy conversion and dissipation can be put to use for the heating of the local surroundings by using light radiation with a frequency that strongly overlaps the nanoparticle SPR absorption band. The intense SPR-enhanced absorption of AuNPs makes the photothermal conversion procedure highly efficient [21, 31, 42].

Photothermal therapy generally employs near infrared (NIR) radiation. The light absorption efficiency of AuNPs in the near-infrared region is high which allows deep tissue penetration. Furthermore, it is possible to avoid the absorbance (Abs) of biomolecules such as hemoglobin [21, 31, 42-43].

Gold nanoparticles have been used with different purposes based on their heating effects under laser irradiation due to the enhanced absorption induced by localized surface plasmon resonance (LSPR). Through the modulation of the geometric and physical

parameters of nanostructures such as shape and size, the plasmon resonance peaks of AuNPs could be tuned to the near-infrared region or the visible region [21, 32, 42-43].

Many researchers have focused on the photothermal therapy of gold nanoparticles with different size and morphology, such as gold nanorods, gold nanostars, gold nanorings, gold nanocages, and hollow gold nanoshells [41].

Since spherical AuNPs exhibit their surface plasmon resonance in the visible region, prospects for in vivo photothermal therapy has become restricted only to shallow depths due to the high tissue absorption at visible wavelengths. Excitation of spherical AuNPs with the appropriate wavelength that overlaps with their plasmon resonance absorption band in the visible range has the advantage of using lower power laser and hence searching for photothermal treatment protocol with the aim of lowering laser power could present a great advantage for achieving selectivity by targeting only tumor cells [21, 31, 42-43].

Moreover, irradiating AuNPs at their plasmon resonance absorption band may require a relatively low concentration of particles to be delivered and consequently prevent possible side effects resulting from high accumulations of nanoparticles at various body organs. The *in vitro* success of photothermal efficiency of AuNPs in the visible range near its plasmon resonance absorption can potentially be extended to in vivo applications of skin and surface type cancers [21, 31, 42-43]. **Figure 8** illustrates what can be possibly the future steps of photothermal therapy.

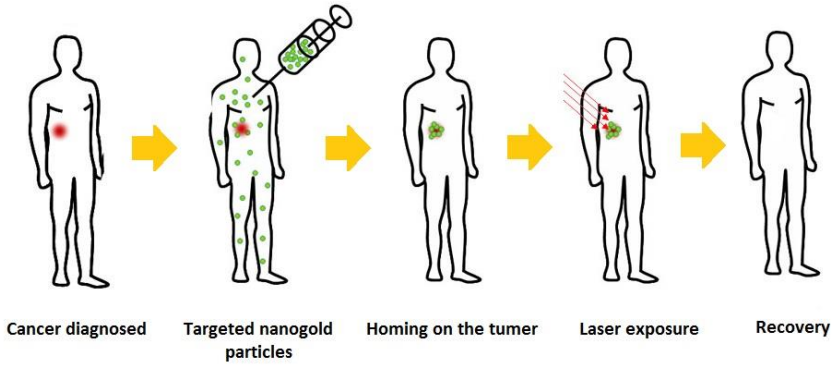

Figure 8: Steps of future photothermal therapy. https://chembites.org/2017/04/26/plasmonic-photothermal-therapy-pptt-using-gold-nanoparticles/ (1/07/2017).

1.5. Scope of the thesis

Therefore, the purpose of the thesis is to perform a photothermal characterization of gold nanoparticles (AuNPs) with a size greater than 14 nm, with the perspective of

downstream application to photothermal ablation of cancer cells. Specifically the following steps are needed:

- Synthesis and characterization of stable and monodisperse gold nanoparticles from 14 nm up to 70 nm in diameter;
- Functionalization with PEG;
- Calorimetry studies in different media;
- Assess the photothermal yield;
- *In vitro* testing.

2. MATERIALS AND METHODS

2.1. Equipment, materials and reagents

Table 2.1: Equipment

Equipment model	Company
UV-Vis Spectrophotometer UV Mini-1240	Shimadzu, Germany
UV-Vis Spectrophotometer Evolution 300	Thermo Scientific, USA
DLS, Nanoparticle Analyzer, SZ-100	Horiba Scientific, Japan
TEM, Hitachi 8100	Hitachi, São Paulo
Fiber coupled laser system fcw 532-8 w	CNI-laser, China
Sigma 3-16K Centrifuge	Sartorius, Germany
Sigma 1-14 Mini-Centrifuge	Sartorius, Germany
Ultrasonic bath S 10 H	Elmasonic, Germany
Shaker GLF 3016	Buch & Holm, Denmark
Infinite M200 Microplate Reader	Tecan, Switzerland
KSV Sigma 702 Tensiometer	Lichfield, United Kingdom
Fortuna 43 Pycnometer	Wertheim. Germany
Differential Scanning Calorimeter Q2000	New Castle, USA

Materials

- Current laboratory material;
- Quartz absorption cell – 105.202-QS (Hellma, Germany);
- Polystirol/Polystirene cuvette (SARSTEDT, Germany);
- Tissue Culture Testplate (96 wells) [SPL LifeSciences);
- Thermocouple (Digital Multimeter);
- Green Laser Pointer (Commercial);
- RC Laser Pointer (Commercial).

Chemical reagents

- Sodium citrate tribasic dihydrate, ≥ 99 % (Sigma-Aldrich, USA), [$HOC(COONa)(CH_2COONa)_2.2H_2O$; MW 294,10 Daltons];
- Gold chloroauric acid 99,999 % (Sigma-Aldrich, USA), [HAuCl4, MW 339.785 Daltons);
- Ultrapure water (18.2 MΩ.cm at 25 °C) [Millipore Corporation, USA], (H_2O, MW 18

Daltons);

- Polyethylene glycol (PEG) [O-(2-Mercaptoethyl)-O'-methyl-hexa(ethylene glycol], (Sigma-Aldrich, USA), [$C_{15}H_{32}O_7S$, MW 356.48 Daltons];
- Sodium Dodecyl Sulfate (SDS) [Sigma-Aldrich, USA, $NaC_{12}H_{25}SO_4$, MW 288.38 Daltons];
- 5,5′-Dithiobis(2-nitrobenzoic acid) [DTNB], (Sigma-Aldrich, USA, $C_{14}H_8N_2O_8S_2$, MW 396.35 Daltons);
- Phosphate buffer (H_4NaO_5P, MW 137.992 Da) - Prepared by the addition of 288.55 mM of Sodium phosphate dibasic (Sigma-Aldrich, USA, Na_2HPO_4, MW 141.96 Da) and 211.45 mM of Monosodium phosphate (Sigma-Aldrich, USA, NaH_2PO_4, MW 119.98 Daltons);
- Phosphate buffer saline ($Cl_2H_3K_2Na_3O_8P_2$, MW 411.029 Daltons);
- MTS (Promega, USA);
- Sucrose (Sigma-Aldrich, USA), [$C_{12}H_{22}O_{11}$, MW 342.30 Daltons).

Media

- Dulbecco's Modified Eagle Medium (DMEM) with color (Phenol red – pH indicator) and without color (Thermo Fisher Scientific, USA);
- Egg white (commercial).

2.2. Synthesis of gold nanoparticles

The optimized protocol of Bastús et al. was used [26]. All glass materials used for the synthesis of AuNPs were previously immersed in *aqua regia* overnight and later washed with Milli-Q water (18.2 MΩ.cm at 25 °C) and desionized water.

1. In a 250 mL round bottom flask, 150 mL of 2.2 mM Sodium Citrate were brought to a boil while in reflux and vigorously stirring during 15 minutes (**Figure 9**);

Figure 9: Synthesis setup.

2. When it starts to boil, it was added 1 mL of 25 mM $HAuCl_4$;
3. The color of the solution changes from yellow to a bluish grey and then to a soft pink in 10 minutes, approximately;
4. The reaction vessel was then cooled down till the temperature of the solution was 90 ºC;
5. 1 mL of 25 mM $HAuCl_4$ was added twice to the solution, in periods of 30 minutes in order to make the seeds;
6. To each generation there is needed 3 additions of chloroauric acid (in a total time of 1h 30 min). The following figure elucidates the process (**Figure 10**);
7. Between generations there is needed a dilution. It was extracted 55 mL of sample to another flask and it was 2 mL of 60 mM Sodium Citrate and 2 mL of ultrapure water.

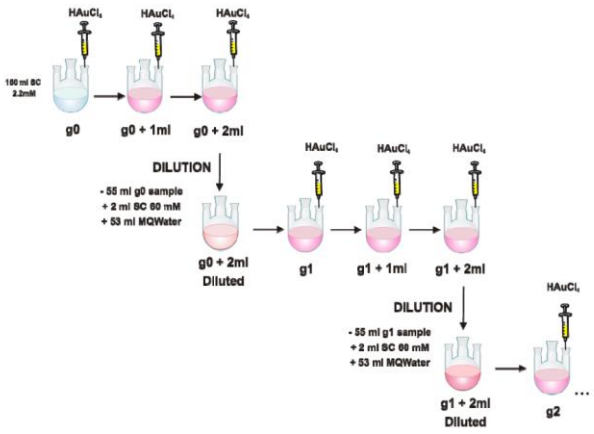

Figure 10: Scheme that sums up the synthesis of different generations of gold nanoparticles [26].

There is a relation between generations, size and concentration of AuNPs (**Figure 11**). The initial aim was to synthesize bigger gold nanoparticles, 30, 60, 90 and maybe 120 nm of diameter, approximately. Note that the concentration of AuNPs does not suffer great fluctuations, according to Bastús *et al* [26].

growth step	diameter (nm)	SD (%)	concentration (NPs/mL)
seeds	8.4 ± 1.0	11.9	3.0×10^{12}
1st	17.6 ± 1.2	6.8	1.9×10^{12}
2nd	22.3 ± 2.2	9.8	1.2×10^{12}
3rd	31.1 ± 2.8	9.0	7.6×10^{11}
4th	36.0 ± 2.4	6.6	4.8×10^{11}
5th	42.2 ± 2.3	7.8	3.1×10^{11}
6th	54.4 ± 3.3	6.1	1.9×10^{11}
7th	64.8 ± 3.4	5.2	1.2×10^{11}
8th	69.3 ± 4.5	6.5	7.8×10^{10}
9th	80.1+ 5.4	6.7	4.9×10^{10}
10th	96.1 ± 5.6	5.8	3.1×10^{10}
11th	109.2 ± 7.6	6.9	2.0×10^{10}
12th	123.6 ± 10.6	8.6	1.2×10^{10}
13th	150.0 ± 9.9	6.6	7.9×10^{9}
14th	180.5 ± 10.7	5.9	5.0×10^{9}

Figure 11: Expected correlation between generations and diameter of gold nanoparticles [26].

2.3. Gold nanoparticles characterization

2.3.1. UV-visible spectroscopy

Several absorbance spectra were taken using a Ultra-Violet – Visible (UV-Vis) spectrophotometer in order to characterize the AuNPs.

2.3.1.1. Haiss et al. approximation

Using the method developed by Haiss et al. [44], it was possible to calculate an approximation of the size in diameter of the AuNPs and its concentration. The following procedure was taken:

- After taking the Absorbance spectrum take note of the values at 450 and 520 nm;
- Calculate the quotient of Abs520/Abs450;
- Substitute the value (y) in the following equation;

$$y = 0{,}335 \ln x + 0.7301 \qquad \textbf{Equation 1}$$

- The value of x corresponds to the approximate diameter of the gold nanoparticles;
- In the table in **Appendix A**, search for the Molar extinction coefficient that corresponds to the calculated diameter;
- Using Lambert-Beer law, calculate the concentration

$$C = \frac{Abs450}{\varepsilon 450}\ x\ dilution\ factor \qquad \textbf{Equation 2}$$

2.3.2. Dynamic light scattering

The hydrodynamic diameter of AuNPs was determined by Dynamic Light Scattering (DLS). The analysis was performed at 25 ºC, with a scattering angle of 90º, using water as medium of dispersion. A volume of 500 µL of AuNPs was first stabilized for 3 minutes and then the samples were measured. DLS analysis was performed at Departamento de Quimica, at the group of Photochemistry (FCT-UNL). During the thesis, a protocol was optimized and it can be seen in **Appendix B**.

2.3.3. Transmission electron microscopy

This was a provided service. Samples of AuNPs were sent to Instituto de Ciência e Engenharia de Materiais e Superfícies (ICEMS/IST), Portugal, for Transmission Electron Microscopy (TEM) analysis. The samples with a volume of 100 µL were deposited in the grids and then air dried. TEM was performed with a HITACHI H-8100 microscope operated at 200 kV.

Particles size and shape were determined by analyzing the TEM pictures in house using the imaging software Fiji.

2.4. Gold nanoparticles functionalization

2.4.1. Functionalization with polyethylene glycol

AuNPs were functionalized with a commercial hetero-functional polyethylene glycol modified with a thiol group at one end. The purpose is to fully saturate the surface of the nanoparticles. The functionalization was done by using the protocol of Conde et al [45].

Firstly, in order to find out the appropriate concentration of PEG to functionalize the nanoparticles, a range of PEG concentrations between 0.001-1mg.mL^{-1} was added to a fixed concentration of gold nanoparticles (10 nM) and SDS (0.028 % (v/v) in aqueous medium. Then, the solutions were incubated for 16 hours at room temperature (RT) with continuous stirring on a shaker. Later, excess PEG was removed by centrifugation (three times, 14,000g, 30 min, and 4 °C) and the supernatants were removed to new tubes and replaced by ultrapure water. The three resultant supernatants were also centrifuged once, in the same conditions, and the level of PEG coverage on the AuNP was evaluated via Ellman's assay, therefore quantifying the yield of the functionalization.

2.4.1.1 Ellman's assay

Ellman's assay is based on the reaction between free PEG's thiol groups presented in the supernatants with DTNB (also known as Ellman's reagent), which results in a yellow solution [46, 47].

The Ellman's reagent reacts with a thiol leading to the formation of a thiol-TNB adduct and a concomitant release of one equivalent of 5-thio-2-nitrobenzoic acid (TNB) [**Figure 12**]. Quantification of the thiols is based on the released TNB which can be measured spectrophotometrically at 412 nm with a molar absorptivity of 14,150 M^{-1} cm^{-1} at a neutral pH [46, 47].

One of the major problems of quantification by spectrophotometry is the interference by compounds which exhibit absorption at the measured wavelength, a phenomenon often encountered with a biological sample and already noticed for the Ellman's spectrophotometric method [46, 47].

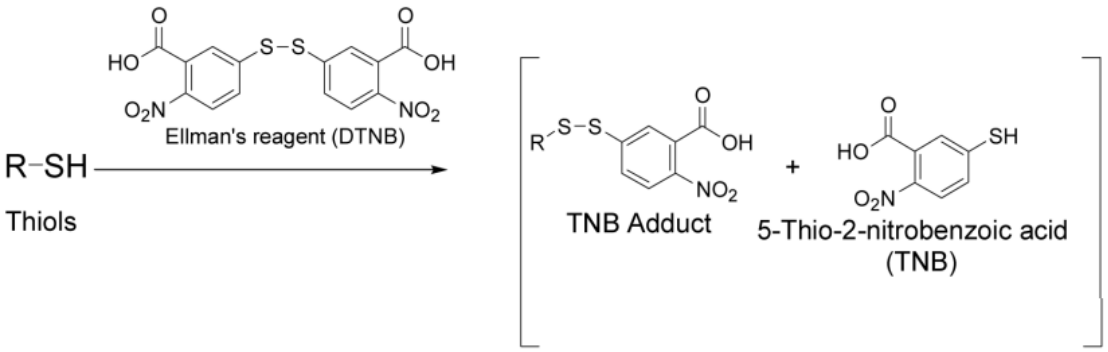

Figure 12: Ellman's assay reaction scheme [46].

For this purpose, on a 96 well-plate, 200 µL of the supernatants, 100 µL of 0.5 M phosphate buffer pH 7.0 and 7 µL of DTNB (2 mg/mL) prepared in 0.5 M phosphate buffer pH 7.0 were mixed. In order to interpolate the absorbance results into PEG concentrations, a calibration curve was also prepared under the same conditions that were described above, but instead of 200 µL of the supernatants, 200 µL of known concentrations of PEG (range of 0-160.5 mg.mL-1) were used. Following 5 min, the absorbance was measured from 290 nm to 600 nm in a microplate reader. Thus, the number of PEG chains that covers 100 % of AuNPs surface were determined.

2.5. Laser irradiation

Using the green laser to irradiate a sample of 200 µL each time, during 180 seconds, with a laser diode intensity (LDI) of 2.7 Amperes, in triplicates, following the manual of good laboratory practice (GLP).

A thermocouple (**Figure 13A**) was used to measure the temperature before and right after the irradiation. The measurement is based on the Seebeck effect (**Figure 13B**). A thermocouple consists of two wires of different metals joined together at one end, called the measurement ("hot") junction. As for the other end, where the wires are not joined, is connected to the signal conditioning circuitry traces, usually made of copper. This junction between the thermocouple metals and the copper traces is called the reference ("cold") junction.

A) **B)**

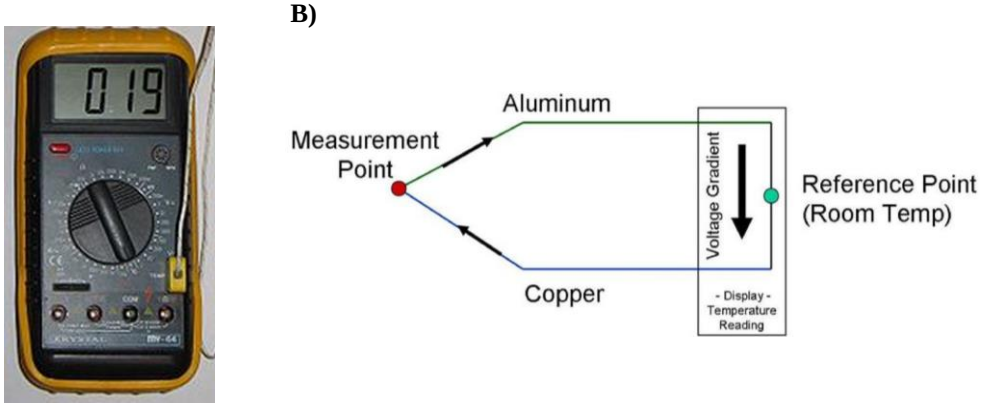

Figure 13: A) Thermocouple used for the calorimetry experiments. B) Principle of measurement of thermocouple (Seebeck effect). http://akeinc.com/news/how-thermocouples-work (15/07/2017)

The voltage produced at the reference junction depends on the temperature at both junctions (measurement and reference). Since the thermocouple is a voltage differential device rather than an absolute temperature measurement device, it is required that the "cold" junction can measure the temperature with great accuracy.

In the end, a ΔΔT is obtained (**Equation 3**). It is a ΔΔT instead of a ΔT because the control is taken into account. The results are also represented as a function of ΔΔT versus concentration because the formula of heat transfer (**Equation 4**) depends of other variables like the mass and the specific heat of the medium.

$$\Delta\Delta T = (Tfinal - Tinitial) - \Delta Tblank \qquad \textbf{Equation 3}$$

$$Q = m\ x\ C\ x\ \Delta\Delta T \qquad \textbf{Equation 4}$$

2.5.1. Water and PBS

A concentration range between 0.1 and 1 nM of AuNPs in water and Phosphate buffered saline (PBS) was used to test the calorimetry. It was used gold nanoparticles with citrate capping (AuNPs@Citrate) and with PEG capping (AuNPs@PEG).

2.5.2. DMEM culture medium (with and without phenol red)

Due to the fact that the medium absorbs a considerable amount of energy, and that was already seen previously, the green laser was used in two modes:

- Continuous Mode (CW)
- Pulsed (3 seconds pulses)

Moreover, these two modes contribute to the production of reactive oxygen species (ROS). However, it is stated in the literature that in continuous mode the amount of produced ROS is much higher (contributing also to the damage of proteins that absorb in the visible, like cytochrome) [49].

The parameters stood the same. The major differences were the concentration of samples used, between 1 nM and 10 nM. It was also used AuNPs@citrate and AuNPs@PEG.

2.5.3. Egg white

Due to the problems with the viscosity of egg white, measures were taken in order to bypass the problem. The eggwhite of an egg was put into a 50 mL falcon (depending on the egg the volume is around 35 mL) and it was added ultrapure water in order to make up a final volume of 45 mL. Finally, a spin was done in the vortex with the purpose of homogenize the solution.

The parameters of measurement were the same as mentioned above. Samples of 200 µL, 180 seconds of irradiation, using an intensity of 2.7 Amperes. The concentrations used were of 4 nM and 10 nM.

2.5.4. Cell culture

The experiment was done with HCT 116 cell line (*Homo sapiens* colon colorectal carcinoma) with the help of MSc. Rita Mendes. In order to do the irradiation in cells, first it must be done a seeding. A determined number of cells, 2E5 cells/mL, were seeded in

colored DMEM media (supplemented) in a 96 well plate (setup in **Figure 14**). Next, this plate is put into a greenhouse at 37 ºC during 24 hours. Then, the middle was carefully withdrawn from each well, leaving the adherent cells in the bottom of the well. Next, 100 µL of DMEM without color (supplemented) was added to the wells that had only cells, and two solutions with the concentration of 10 nM of AuNPs with different cappings (Citrate and PEG) in DMEM without color (supplemented) were added.

The plate was then put into a greenhouse at 37 ºC. Then, after 2 hours of incubation, the middle was withdrawn and replace with fresh DMEM media. The irradiation was done using the same parameters as before, but only in continuous mode.

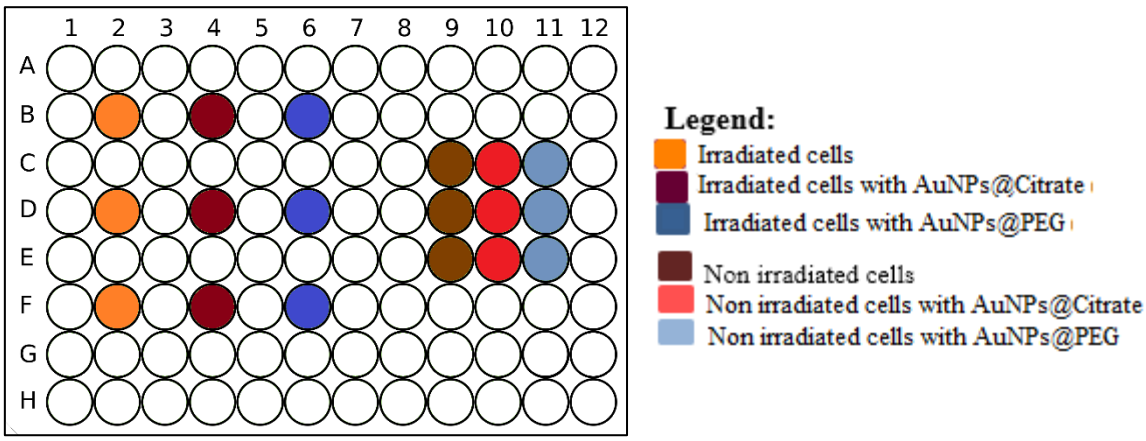

Figure 14: Setup of each 96 well plate.

2.6. Assessment of cell viability

2.6.1. MTS assay

MTS assay is a very sensitive colorimetric method to assess metabolic activity, as well as being used as a cytotoxic assay. It can be used to infer the number of viable cells. MTS tetrazolium salt is reduced into formazan, a converted aqueous, soluble product by dehydrogenase enzymes present in metabolically active cells (**Figure 15**) [50]. The quantity of formazan produced is directly proportional to the number of viable cells and so, the cell viability can be obtained according to the following formula:

$$Viability\ (\%) = \frac{mean\ of\ Abs\ of\ treatment\ group}{mean\ of\ Abs\ of\ control\ group}\ x\ 100 \qquad \textbf{Equation 5}$$

The MTS assay was done with the help of MSc. Rita Mendes.

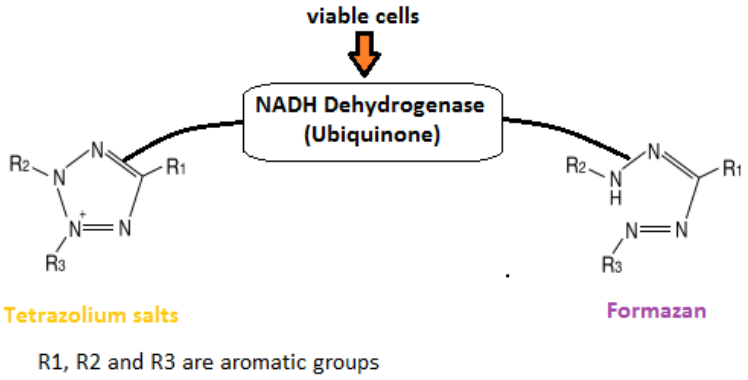

Figure 15: Principle of MTS assay. Tetrazolium salts (yellowish color) are reduced to formazan (purplish color) by NADH Dehydrogenase (complex I of respiratory chain) in the presence of metabolic active cells.

2.7. Size and shape separation of gold nanoparticles

In order to reduce the polidispersivity of the synthesized gold nanoparticles throughout size and shape separation, a protocol was done based on the experiments of Wu et al. and Kumar et al (**Figure 16**) [50, 51]:

- Prepare a centrifugation tube of 2 mL with 4 layers of sucrose (30% - 60%);
- Insert 200 uL of AuNPs;
- Centrifuge to 4000g during 20 minutes;
- 4 fractions were obtained;
- Separate each fraction in a different tube;
- Centrifuge each fraction to 30000g during 5 minutes in order to remove the sucrose;
- Ressuspend in a 0.1 % solution of SDS.

This process is called density gradient centrifugation. This work was done with the help of PhD Fábio Carlos, PhD Bruno Veigas and MSc. Rita Mendes.

A size separation can also be done (but was not performed during this work):

- Insert each fraction in a well of a 0.9 % Agarose gel in 1x TBE buffer (pH = 9);
- Run the gel for 1 hour at 100 V:
- Cut the bands separately;
- Dissolve each one in Milli-Q water at 90 ºC;
- Centrifuge at 9000 g for 5 minutes to remove the agarose;
- Ressuspend in 1 mL of ultrapure water to post-characterization.

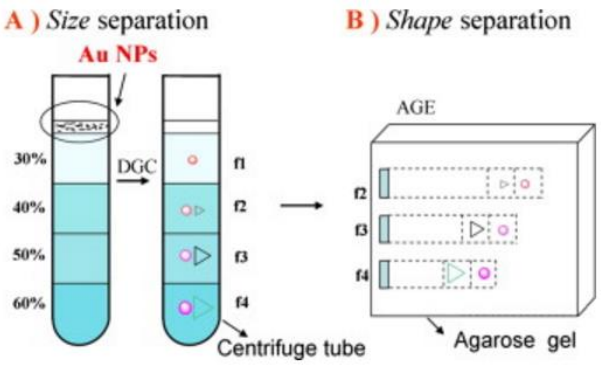

Figure 16: Elimination of polidispersivity: size (A) and shape (B) separation of gold nanoparticles [50].

2.8. Density measurement

The density (ρ) is an elementary physical property of matter. It is stated, for a homogeneous object, that the density is defined as the ratio of its mass m to its volume V. It is influenced by the thermal expansion of materials, as well as its physical state. For liquids, the 2 of the most popular methods of density measurement are:

- Tensiometer
- Pycnometer

2.8.1. Tensiometer

The density of PBS, DMEM (with phenol red) and DMEM (without phenol red) was measured using samples of 25 mL with a KSV Sigma 702 Tensiometer (**Figure 17**).

The concept of measurement is based on the Archimedes' principle. Using a sphere attached to a cable (with known mass), and immersing it on a liquid of known volume, it is possible to calculate the density, knowing that the mass of the sphere is different when submerged in the liquid.

The analysis was performed at Departamento de Quimica (FCT-UNL) with the help of Professor João Sottomayor.

Figure 17: Used tensiometer to assess the densities of the different media.

2.8.2. Pycnometer

The density of PBS, DMEM (with phenol red) and DMEM (without phenol red) was measured using samples of 25 mL with a Fortuna 43 Pycnometer. The pycnometer (or specific gravity bottle) [**Figure 18**] is a glass flask with a close-fitting ground glass stopper with a fine hole through it, that enables the measurement of density with great accuracy. The needed steps are as following (the weightings were done in triplicate):

- Weight the empty pycnometer;
- Fill the pycnometer with distilled water;
- Weight the pycnometer;
- Know we know the mass of water inside de pycnometer ($m1$):
- Check the temperature (checking a table, you know $\rho 1$):
- Dry very well the pycnometer, use compressed air and acetone;
- Fill the pycnometer with the unknown sample;
- Weight the pycnometer.
- Know we know the mass of the liquid inside the pycnometer ($m2$).

So, equalizing the volumes (25 mL), we know the density.

$$\frac{m1}{\rho 1} = \frac{m2}{\rho 2}$$

The assessment was performed at Departamento de Quimica (FCT-UNL) with the help of Professor João Sottomayor.

Figure 18: Pycnometer used for measuring the densities of the different media.

2.9. Differential scanning calorimetry

The specific heat (Cp) of PBS, DMEM (with phenol red) and DMEM (without phenol red) was assessed using a Differential Scanning Calorimeter. In order to perform that analysis, the following steps are needed:

1) Weight the pan (**Figure 19a**) in an analytical balance (one with 5 decimal places);
2) Insert a drop of the sample (one medium at a time) in the pan;
3) To know the exact weight of the sample, seal the pan with a sealing press (**Figure 19b**);
4) Introduce the pan in the Calorimeter (**Figure 19c**). The reference pan is already inserted (**Figure 19d**);
5) Insert the data obtained through the weighting (pan and sample masses) and the following parameters in the Calorimeter:

1: Sampling interval 0.10 s/pt

2: Data storage On

3: Equilibrate at 40.00 °C

4: Ramp 1.00 °C/min to 20.00 °C

5: Isothermal for 1.00 min

6: Mark end of cycle 1

7: Ramp 1.00 °C/min to 30.00 °C

8: Isothermal for 1.00 min

9: Mark end of cycle 2

10: Ramp 1.00 °C/min to 20.00 °C

11: Isothermal for 1.00 min

12: Mark end of cycle 3

13: Ramp 1.00 °C/min to 30.00 °C

14: Isothermal for 1.00 min

15: Mark end of cycle 4

16: Ramp 10.00 °C/min to -50.00 °C

17: Isothermal for 1.00 min

18: Mark end of cycle 5

19: Ramp 10.00 °C/min to 40.00 °C

20: Isothermal for 1.00 min

21: Mark end of cycle 6

22: Equilibrate at 40.00 °C

23: Data storage Off

The measurement was performed at Departamento de Quimica (FCT-UNL) in the laboratory of dielectric relaxation spectroscopy and differential scanning calorimetry, with the help of Professor Madalena Dionísio and PhD Teresa Cordeiro.

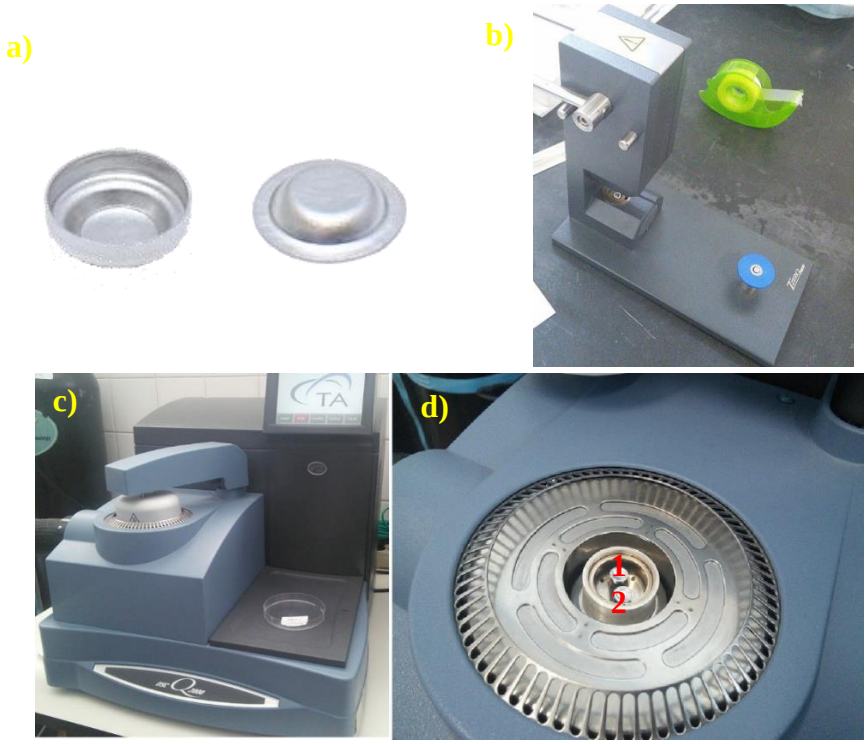

Figure 19: a) An exemplar of a pan used in Differential Scanning Calorimetry. b) Hydraulic press used to close the lids. c) Used Differential scanning calorimeter to calculate the specific heat of the different media d) Place where are inserted the pans: 1 – Reference pan 2 – Sample pan.

3. RESULTS AND DISCUSSION

3.1. Gold nanoparticles

Generally, gold nanoparticles are synthesized in water by the chemical reduction of Au^{3+} derivatives to neutral gold atoms (Au^0), using a reducing agent. There is also a need of a capping and/or stabilizing agent in order to prevent the aggregation of the particles, and also to control the growth and size of nanoparticles [9, 20, 22].

The growth of nanoparticles involves 2 steps: the "Focusing period", where the mean radius of the particles increases and the size distribution narrows, and the "Ostwald ripening", which is characterized by the increase of heterogeneity of sizes in the solution. Factors like temperature, ionic strength, time of the reaction and the stoichiometry of reactants and its order of addition determine the size of AuNPs [26].

There are many different protocols for the synthesis of gold nanoparticles. However, the simplest one available was established by Turkevich *et al.* in 1951 (based on work done by Faraday) and refined by Frens in the 1970s. This method allows the synthesis of monodisperse and spherical gold nanoparticles with a size around 10 - 20 nm in diameter. It uses a gold salt, chloroauric acid ($HAuCl_4$) and sodium citrate as both reducing and capping agent [9, 20, 22].

Larger particles can be produced with the previous reactants. If the amount of added sodium citrate is diminished, the amount of the citrate ions available for stabilizing the particles is lower, leading to the coalescence of the small particles still present in solution, until the total surface area of all particles becomes small enough to be covered by the existing citrate ions. This all come with a price, the sacrifice of the monodispersity and the shape of the AuNPs. That is why it is used more than 1 reducing agent (e.g. hydroquinone) [9, 20, 22].

In the present work, the method developed Bastús et al. was used to produce big and stable AuNPs. The reactants are exactly the same as the Turkevich method, but the order of addition is different. First, the sodium citrate is heated and then the gold is added. Keeping the temperature at 90 ºC and adding the gold at a steady rate allows the shift of the equilibrium of the reaction to the focusing period and leads to the formation of bigger nanoparticles (through the formation of oval particles and the nucleation of the smaller ones) [26].

3 synthesis were performed. In the next figure (**Figure 20**), it is possible to discern

different generations of the first synthesis.

Figure 20: Different generations of the first synthesis of gold nanoparticles (from left to right: G0, G1, G2, G3 and G4).

It is important to outline that the second and third synthesis were used to do the experimental work.

3.2. Characterization of gold nanoparticles

3.2.1 UV-visible characterization

The colloidal solutions of gold nanoparticles were characterized by the use of Ultraviolet-Visible (UV-Vis) spectroscopy, Dynamic Light Scattering (DLS), and Transmission Electronic Microscopy (TEM).

Like stated before, the LSPR is a very important optical property of AuNPs. By performing analysis of the SPR absorption band, important information can be extracted about the particles, such as their size, shape, concentration and dispersion state, thus making this technique a valuable tool for the characterization of these nanomaterials [52]. In the next figure (**Figure 21**), it is possible to perceive the spectra of the different generations of AuNPs of the second synthesis.

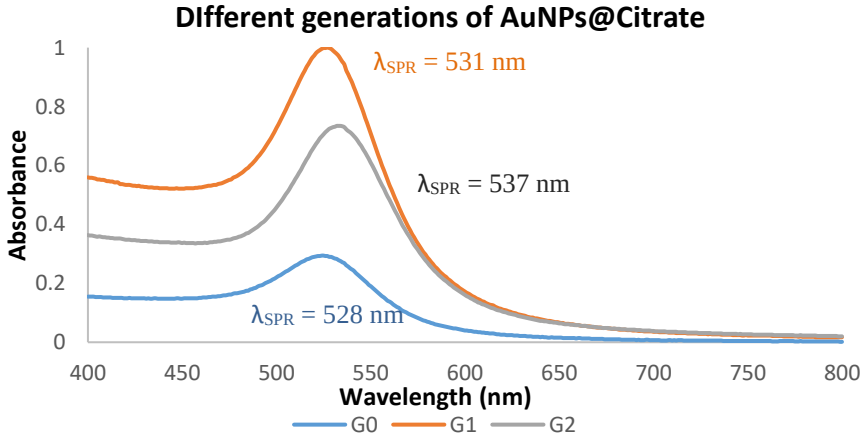

Figure 21: Absorbance spectra of the different generations (G0, G1 and G2) of gold nanoparticles.

By the position and width of the SPR band it is possible to conclude that there is a good monodispersivity in AuNPs. However, it presents a great heterogeneity of sizes. It is important to state that according to literature, AuNPs with a size in diameter between 5 and 30 nm have a SPR peak band centered at 520 nm [53]. It is possible to see in **Figure 21** that the SPR peak suffers a red-shift as size increases (from G0 to G2), confirming what was proclaimed above.

Anisotropy can also be observed by looking to the colloidal solutions at the naked eye, the solutions tend to gain a milky appearance, due to the fact that the scattering of light is different in each direction.

3.2.2. Dynamic light scattering characterization

DLS is also used for AuNPs characterization. Using this technique, we can measure the variation of scattered light of AuNPs according to their Brownian motion, thus obtaining an approximate measure of their size. Brownian motion results from the collision of the solvent molecules (in this case, water) with the nanoparticles, causing them to move randomly. The velocity of the movement is defined by the translational diffusion coefficient and the AuNPs' size calculated from hydrodynamic diameter (HD). Factors like temperature, ionic strength and concentration of the samples are important for the achieved results [54, 55]. The **equation 6** is the Stokes-Einstein equation. It is used to calculate the diffusion coefficient (D), using the Boltzman constant (k = **1.38E-23 J.K^{-1}**), the temperature (T) and the viscosity (η) of the medium, the hydrodynamic radius (R). It assumes that all particles are spherical.

$$D = \frac{kT}{6\pi\eta R} \qquad \textbf{Equation 6}$$

DLS analysis also provides information about the AuNPs' size distribution through the polydispersity index (PI) [54]. In the next graphic, a dispersion of sizes for each generation of AuNPs can be seen, and an increase of the mean size with the increase of generation as it was expected (**Figure 22**).

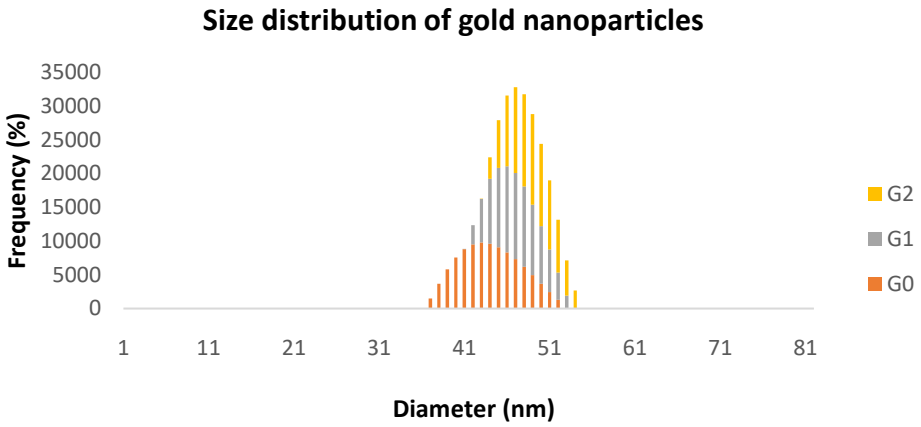

Figure 22: Size dispersion of the different generations (G0, G1 and G2) of gold nanoparticles determined through Dynamic Light Scattering.

3.2.3 TEM characterization

Transmission electron microscopy is a technique used to observe and characterize the different features of very small specimens with very fine detail. Instead of light it uses a beam of electrons providing, therefore, higher magnification and greater resolving power. An image is formed from the interaction of the electrons transmitted through the specimen; the image is magnified and focused onto an imaging device. Hence it provides information about the morphology, composition and crystallographic structure of samples [56]. It is possible to see a TEM image of each generation of particles, with the same resolution (**Figure 23**).

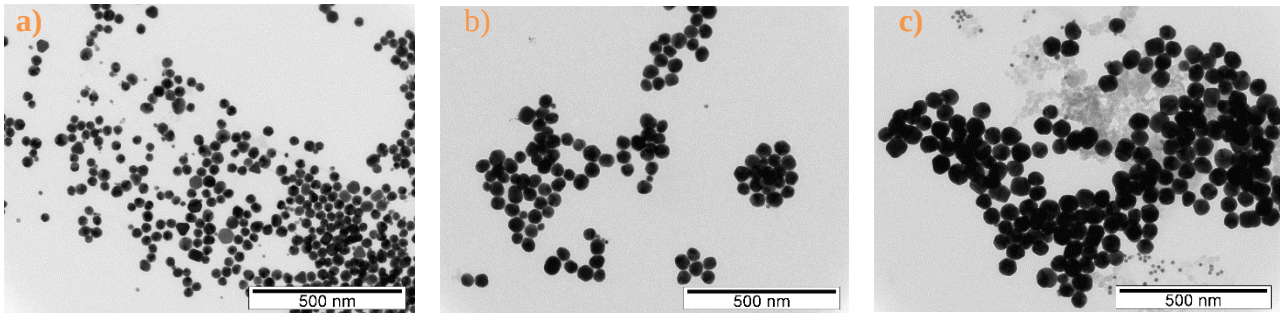

Figure 23: TEM images of different generations of gold nanoparticles: a) G0 b) G1 c) G2.

The following table, summarizes the results (**Table 3.1**). The Haiss et al. approximation does not show coherent results in comparison with DLS and TEM. This happens because it assumes that all AuNPs are spherical and monodisperse. As for the DLS, the PI is higher than 0.2, which means that polidispersivity is present in the solutions, corroborating what was already observed in the absorbance spectra.

Table 3.1: Summary of the results given by all the different techniques used to characterize the gold nanoparticles.

	Haiss et al.		DLS		TEM
	d (nm)	C (M)	d (nm)	PI	d (nm)
G0	39.5	2.33E-10	38.4 ± 0.25	0.29 ± 0.14	32.84 ± 6.93
G1	29.7	1.87E-09	47.5 ± 0.65	0.26 ± 0.08	47.02 ± 7.39
G2	40.6	4.45E-10	55.2 ± 1.3	0.3 ± 0.1	53.14 ± 16.31

3.3. Scattering and absorption with different lasers

It was experimented in a solution of gold nanoparticles using two different lasers: green and red. The purpose was to see what happened to which one, in which situation will occur scattering and/or absorbance (**Figure 24**).

As it was expected, using the green laser it is mainly present absorption, with some reflection, probably to the glass. This is because the plasmonic of AuNPs is situated the region of the green. On the other hand, when exposing the same AuNPs to the red light, scattering is predominant.

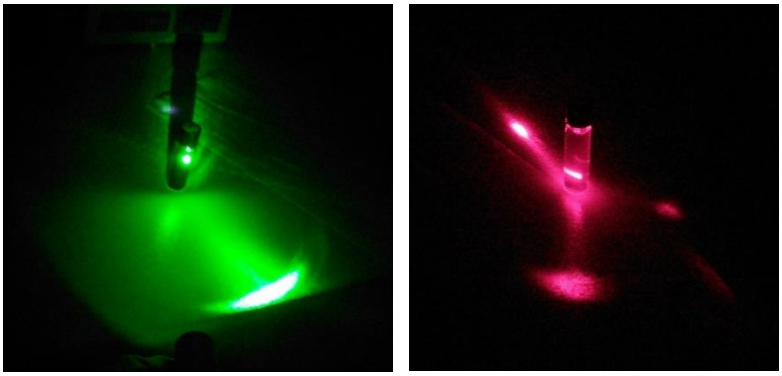

Figure 24: HPLC tube containing the same gold nanoparticles exposed to green and red light.

3.4. Functionalization and characterization

The AuNPs were functionalized with PEG, in order to increase their stability and their biocompability within the human body. The AuNPs initial capping agent, citrate, was replaced by PEG molecules with a thiol group at one end to be attached to the AuNP core. It was used a PEG coverage of 100 %, corresponding to a concentration of 0.1

mg.mL^{-1} in the bigger gold nanoparticles that were previously synthesized. According to literature, 100% coverage allows the attainment of a higher photothermal conversion [57]. As for 15 nm AuNPs@Citrate, the concentration that has to be used to a fully covered particle is 0.01 mg.mL-1. Adding moieties of PEG to the surface of the particles increases its size, and that can be seen in UV-vis spectrum. Comparing both spectra, it is possible to visualize a small red shift (approximately 2 nm) [**Figure 25**]. This is corroborated by literature [57].

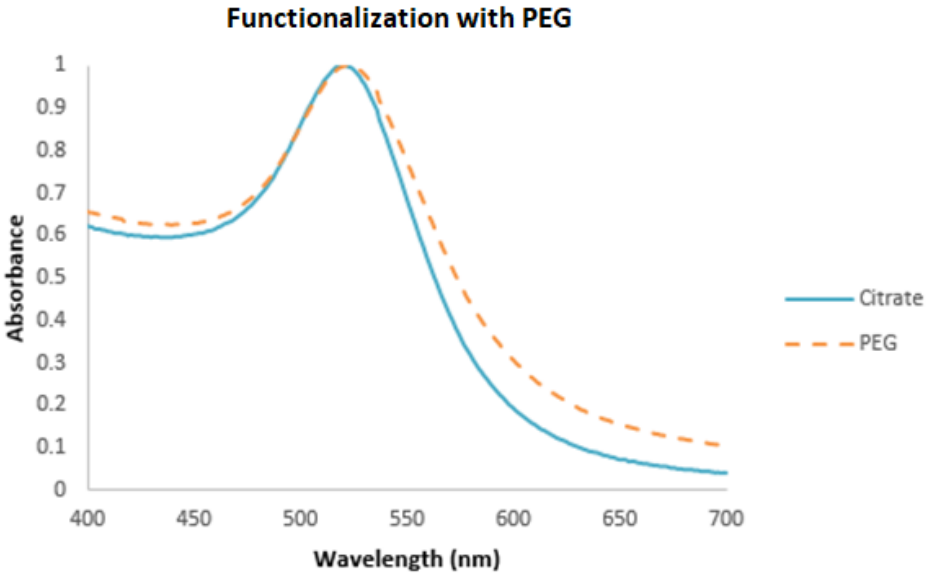

Figure 25: Absorbance spectra of gold nanoparticles with a citrate and PEG capping.

3.5. Stability of gold nanoparticles

When dilluting AuNPs in water, they tend to unstabilize due to the fact that the internuclear space between them increases as well as its diffusion coefficient. That is why AuNPs with a citrate capping could aggregate. This can be proven by a flattening in the SPR band.

Moreover, if there is a variation in the ionic strength or in pH, nanoparticles also tend to aggregate. This happens because there is a change in the dielectric of the medium. When this occurs, the negative charge of the surface provided by the citrate is overridden and they tend to coalesce.

In "PEGylated" gold nanoparticles, a stability test was performed in order to perceive their stability in PBS. Previous studies were done using 15 nm AuNPs@PEG and they did not aggregate. However, using these particles (that were synthesized by a seeding method), aggregation occurs. In fact, according to literature "PEGylated" gold

nanoparticles are not stable [30].

In the following graphic, it is possible to see different dilutions in PBS and a control. They immediately aggregate (**Figure 26**).

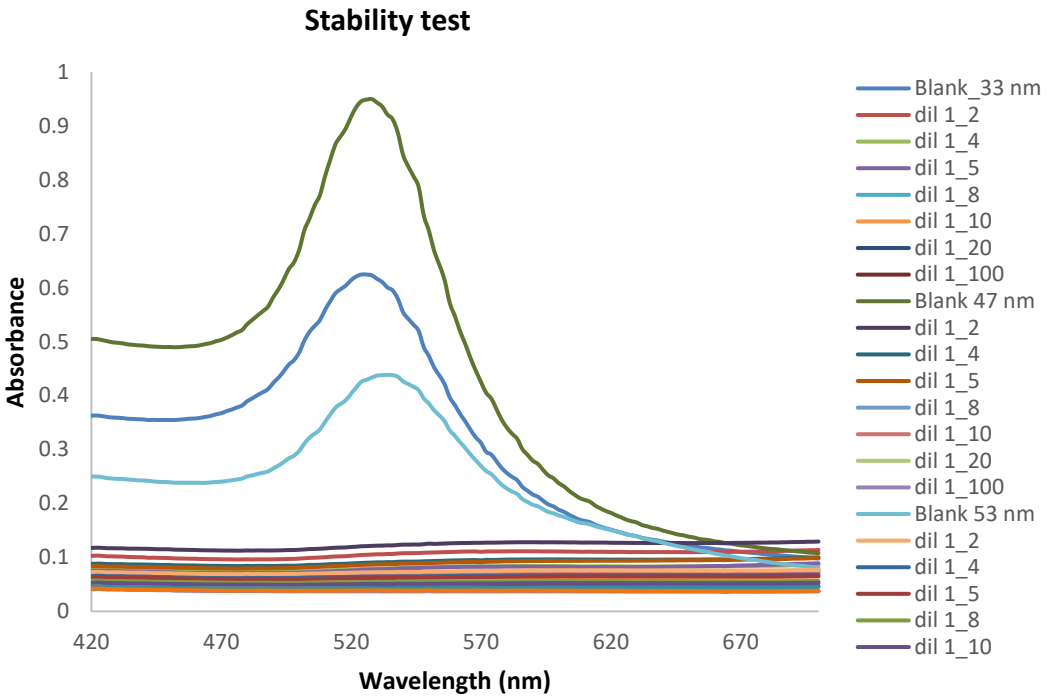

Figure 26: Stability test of "PEGylated" gold nanoparticles in PBS using different dilutions.

3.6. Calorimetry

3.6.1. Water

Most of our body is water, about 70%. It is stable, inert, being part of most buffers and culture media. Thus, it is the perfect medium to start calorimetry experiments.

3.6.1.1 Behavior of citrated capped nanoparticles in water

Firstly, using water as a medium to heat the AuNPs, the results showed a small increase of temperature. This also happens due to the fact that the concentration of AuNPs is not very high (1 nM or lower). Comparing the results of the 3 sizes, we can conclude that the smaller gold nanoparticles have a higher photothermal conversion capability (**Figure 27**).

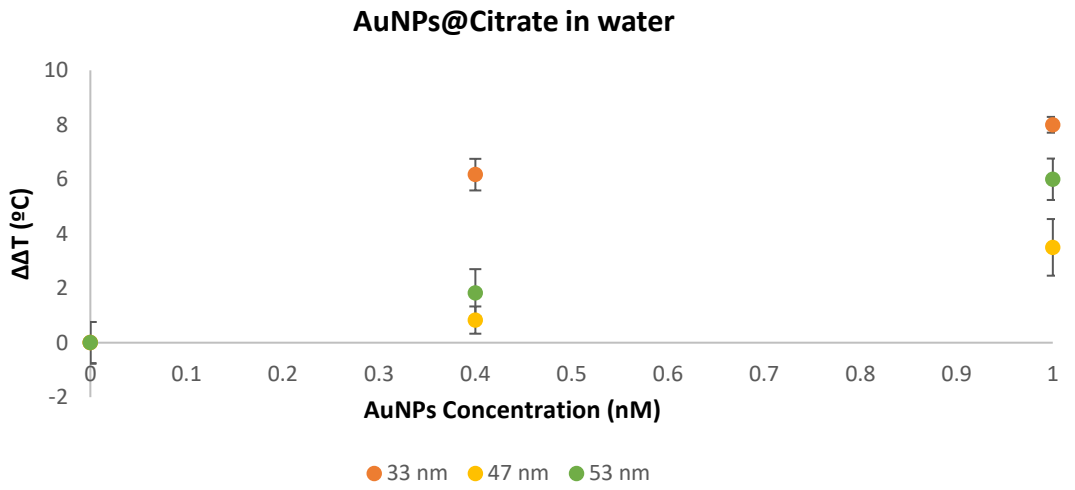

Figure 27: Calorimetry results of citrate capped gold nanoparticles with a concentration of 0.4 nM and 1 nM in water.

3.6.1.2 Behavior of "PEGylated" gold nanoparticles in water

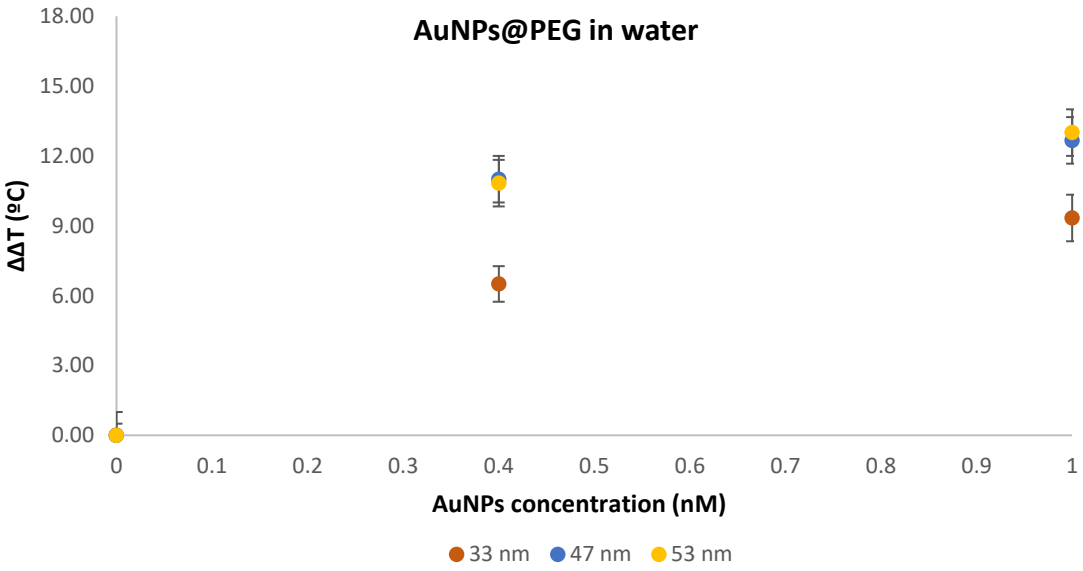

Figure 28: Calorimetry results of "PEGylated" gold nanoparticles with a concentration of 0.4 nM and 1 nM in water.

Comparing the spectra of gold nanoparticles with different cappings (citrate and PEG: **Figures 27** and **28**, respectively), it is possible to observe that the "PEGylated" gold nanoparticles have a more efficient photothermal conversion, and this was not expected because when using PEG, the core is less accessible than by comparing with particles with citrate covering. Being less accessible, it is expected that it will convert less energy into heat. Another explanation that can be given is that the scattering cross section of the particles when the nanoparticles have a PEG capping is lower.

It was expected that the smaller particles (33 nm) had a higher photothermal conversion capacity, but the results do not show that. A possible explanation can be made if there is a great dispersion of sizes, which is the case. When attempting to functionalize with 100% of PEG, if there a great heterogeneity of sizes, the smaller particles are more "PEGylated" than the bigger ones. If these happens, that could be an explanation for not achieving the expected results.

3.6.2. PBS

PBS is a buffer commonly used in biological research. Due to the fact that it has salt, it affects the dielectric constant of a medium, so the gold nanoparticles tend to aggregate (**see subsection 3.5**).

3.6.2.1 Behavior of citrated capped gold nanoparticles in PBS

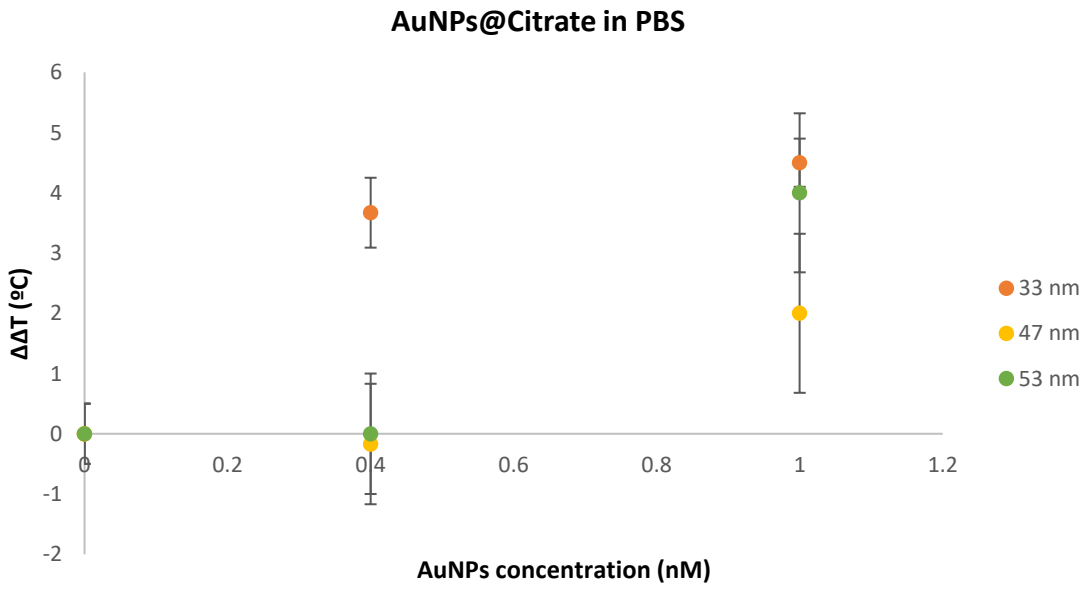

Figure 29: Calorimetry results of citrate capped gold nanoparticles with a concentration of 0.4 nM and 1 nM in PBS.

The results (**Figure 29**) show a heating capability of AuNPs even lower than in water, and that was expected. If the particles are aggregating, the scattering component increases dramatically. And the scattering does not contribute to an increase of heat of the media [58].

Furthermore, the standard deviation (SD) is higher than normal, this can be explained by the fact that the AuNPs are aggregating, but this is not an instantaneous

process, it is a continuous process, making the variations of temperature higher than normal.

3.6.2.2 Behavior of "PEGylated" gold nanoparticles in PBS

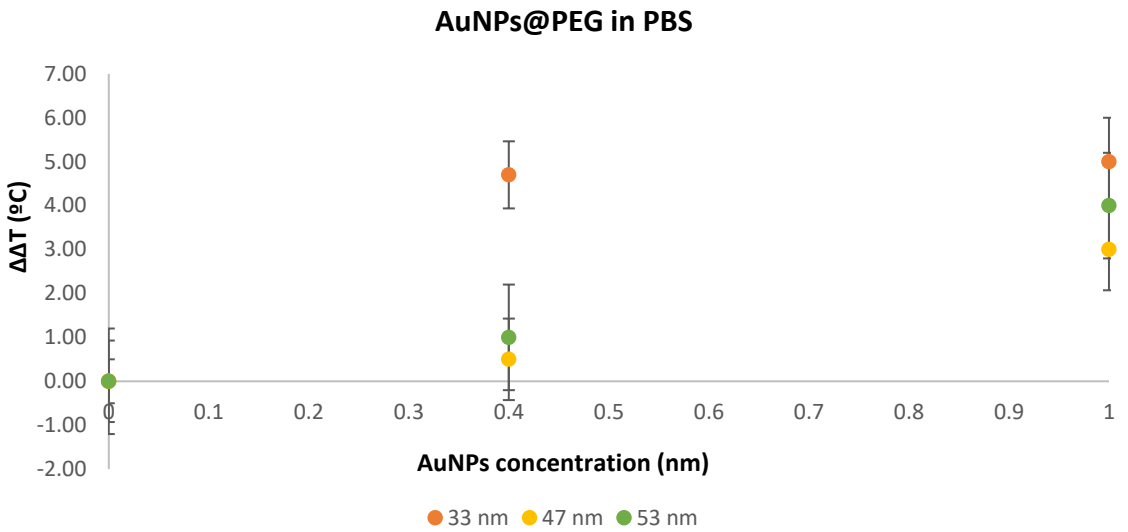

Figure 30: Calorimetry results of "PEGylated" gold nanoparticles with a concentration of 0.4 nM and 1 nM in PBS.

By using, "PEGylated" gold nanoparticles in PBS, and knowing that they are not stable in this medium, the expected results were matched. Even though, the increase of heat was higher than in citrate capped gold nanoparticles (**Figure 30**).

3.6.3. DMEM

DMEM is a medium used for the growth of a mammalian cells. It has 2 variations, one with a pH indicator (phenol red) which has a reddish color, and the other without a pH indicator (almost without color).

Due to the fact that the increase of temperature was not significant, the concentration of gold nanoparticles was increased 10 times. Also, 2 modes of the laser were tried: continuous and pulsed. Due to the fact that the media absorbs a considerable amount of energy, especially the DMEM with phenol red, having the same color as the particles, they absorb the same wavelengths. This could mean a possible synergy, potentiation or additivity. Or in the other hand, they can interfere with each other. It is stated in literature that the 2 media lead to the production of reactive oxygen species, but by using pulses of energy, the produced ROS are much lesser.

3.6.3.1 Behavior of citrated capped gold nanoparticles in DMEM (with phenol red)

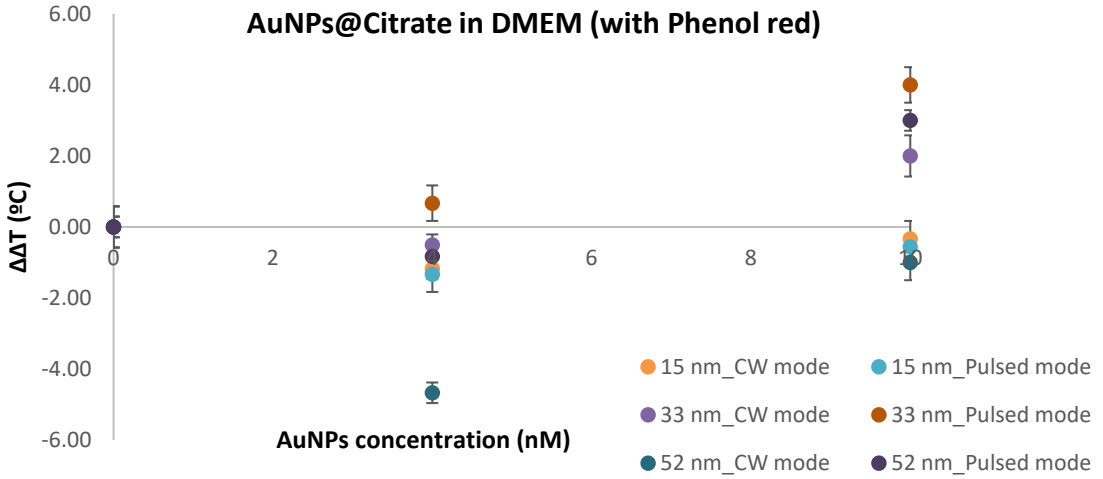

Figure 31: Calorimetry results of citrate capped gold nanoparticles with a concentration of 4 nM and 10 nM in DMEM (with phenol red), using the laser in continuous and pulsed mode.

Due to the fact that the particles with 47 and 53 nm showed similar results, another size of AuNPs was attempted: 15 nm particles. These particles are commonly used in the laboratory. They were produced by using the Turkevich method [18] by Raquel Vinhas and Fabio Carlos.

By looking the results (**Figure 31**), it is possible to see that the DMEM has great interference with the particles. The AuNPs also aggregate, increasing a lot the scattering component of the AuNPs. And as it was already stated, the scattering does not contribute to the increase of heat. One possible explanation for the negative results is the competition between the AuNPs and the phenol red for the absorbance of light (resulting in an antagonistic effect).

Focusing in the results of the pulsed mode, the results were much better – positive ΔΔT were achieved. AuNPs with 33 nm showed higher photothermal conversion capabilities, instead of the AuNPs with 15 nm because these last ones aggregated (**Figure 32**).

Figure 32: Citrate capped gold nanoparticles in DMEM (phenol red): a) monodisperse (33 nm) b) aggregated (15 nm).

3.6.3.2 Behavior of "PEGylated" gold nanoparticles in DMEM (with phenol red)

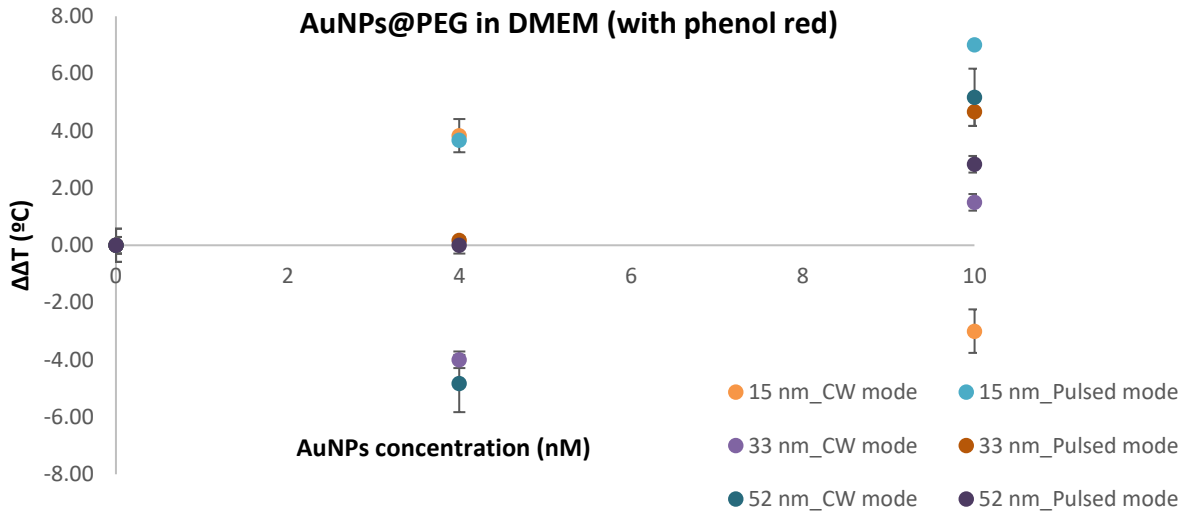

Figure 33: Calorimetry results of "PEGylated" gold nanoparticles with a concentration of 4 nM and 10 nM in DMEM (with phenol red) , using the laser in continuous and pulsed mode.

Even though the capping of the gold nanoparticles was changed, the interference of the phenol red in the photothermal conversion of the AuNPs did not cause great changes. Therefore it is not possible to take significant conclusions from the results by using continuous mode (**Figure 33**).

15 nm AuNPs@PEG did not aggregate, thus achieving a higher photothermal conversion in this media (in the pulsed mode), like it was expected, smaller particles have a higher photothermal conversion capability [33, 59].

3.6.3.3 Behavior of citrated capped gold nanoparticles in DMEM (without phenol red)

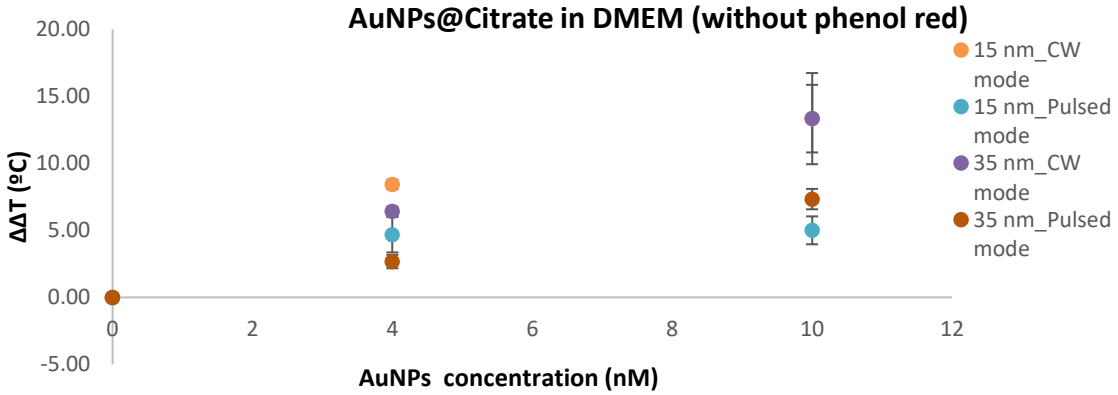

Figure 34: Calorimetry results of citrate capped gold nanoparticles with a concentration of 4 nM and 10 nM in DMEM (without phenol red), using the laser in continuous and pulsed mode.

Only 2 different sizes were used in the experiments that used DMEM without phenol red as a substract for calorimetry. The obtained results showed a slightly higher photothermal conversion capacity of 15 nm AuNPs@Citrate, in the continuous mode. As for the pulsed mode, the AuNPs have approximately the same photothermal conversion efficiencies. It could be interesting to see how this situation would evolve if the concentration is increased.

3.6.3.4 Behavior of "PEGylated" gold nanoparticles in DMEM (without phenol red)

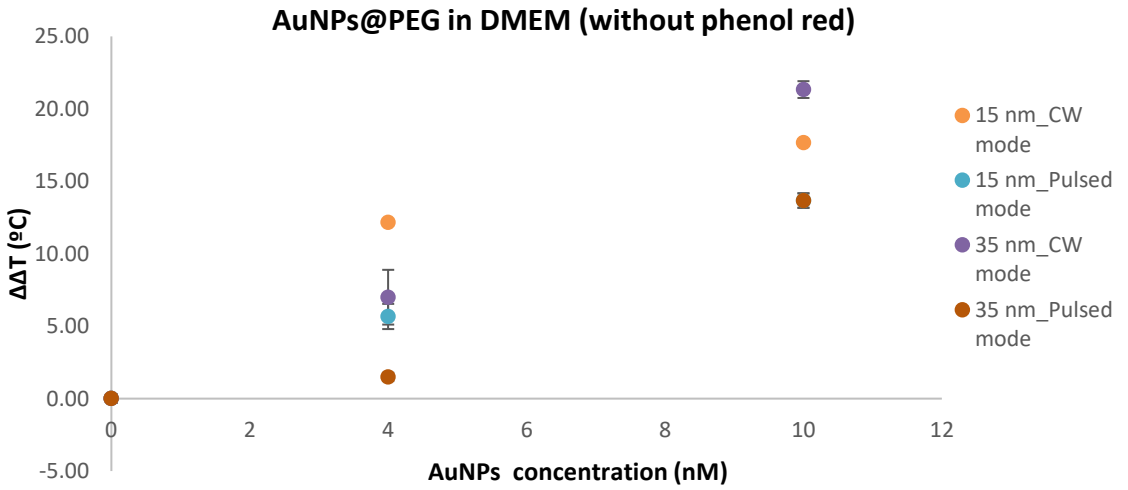

Figure 35: Calorimetry results of citrate capped gold nanoparticles with a concentration of 4 nM and 10 nM in DMEM (without phenol red), using the laser in continuous and pulsed mode.

Comparing the results between the AuNPs with a capping of a citrate and a capping of PEG (**Figures 34** and **35**), these last ones present a higher photothermal conversion capacity, like it was previously seen. Using continuous mode, higher temperatures were attained, due to the fact they have a higher time of exposure.

3.6.4. Egg white

Egg white is used as a cell culture system. Due to the fact that possesses a lot of protein that are homologous or even the same that are present in the human body, it is a good medium to test the stability and the photothermal activity of gold nanoparticles.

3.6.4.1 Behavior of citrated capped gold nanoparticles in egg white

The calorimetry results of AuNPs in egg white are in accordance to what was

expected. “PEGylated” gold nanoparticles are more efficient at converting radiation into heat than AuNPs@Citrate. Moreover, the smaller nanoparticles (15 nm) achieved better results too (in pulsed and continuous mode) [**Figures 36** and **37**].

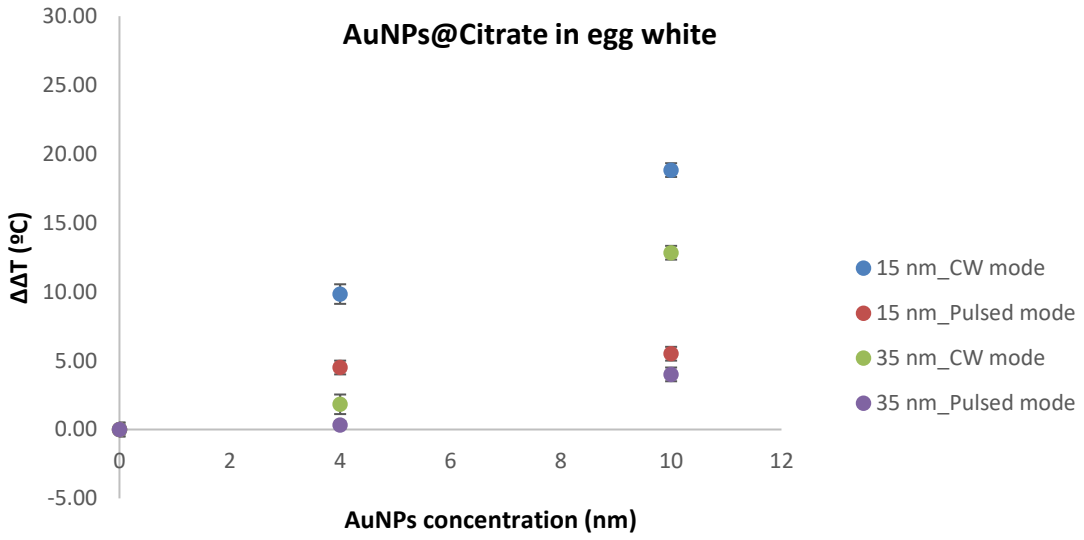

Figure 36: Calorimetry results of citrate capped gold nanoparticles with a concentration of 4 nM and 10 nM in egg white, using the laser in continuous and pulsed mode.

3.6.4.2 Behavior of “PEGylated” gold nanoparticles in egg white

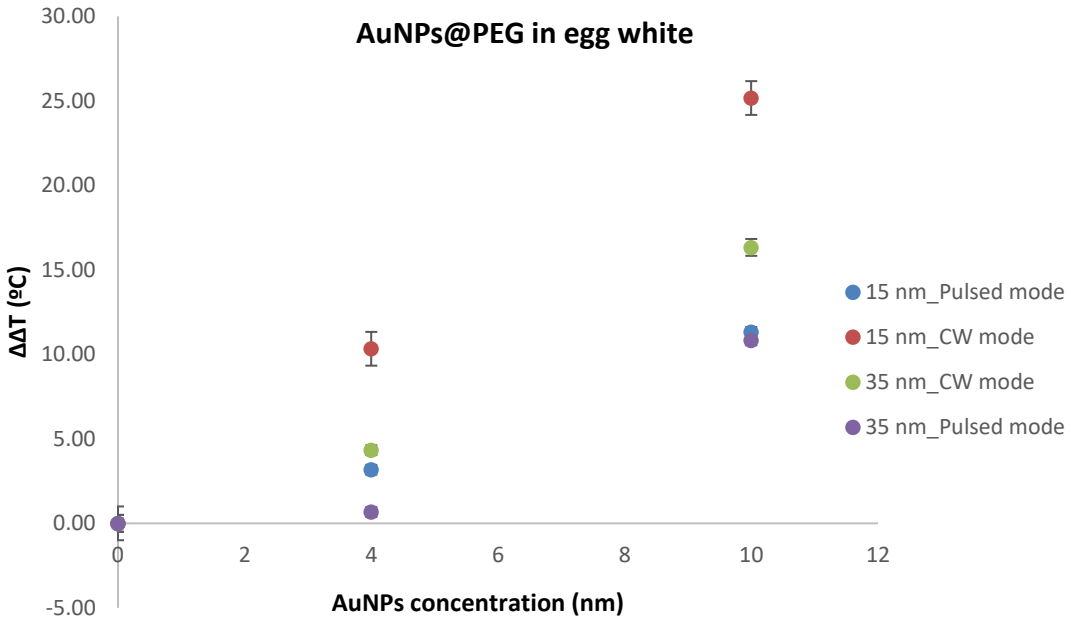

Figure 37: Calorimetry results of “PEGylated” gold nanoparticles with a concentration of 4 nM and 10 nM in egg white, using the laser in continuous and pulsed mode.

3.6.5. Before and after irradiation

Comparing (by using UV-vis spectroscopy) the changes in the spectra of different AuNPs before and after the experiments of calorimetry was also done. In the following spectra (**Figure 38**) it is possible to observe that there are no visible changes in any of the gold nanoparticles. Therefore, it is possible to conclude that are no structural changes in the particles during the assays.

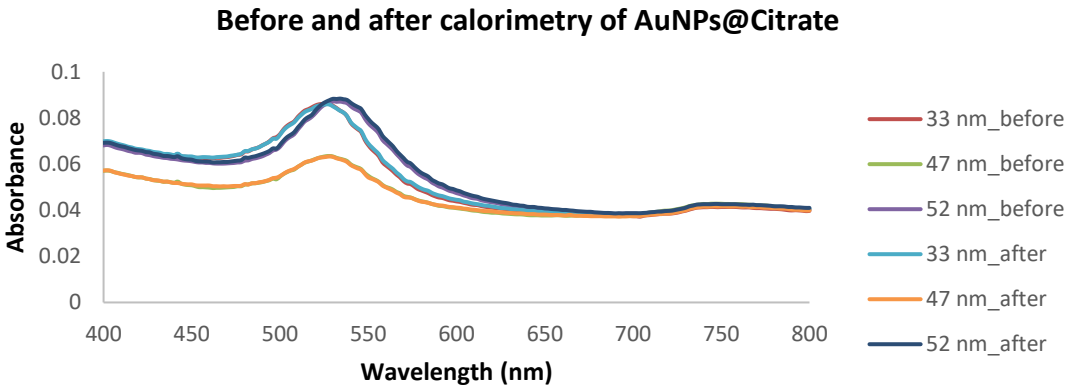

Figure 38: Absorbance spectra of gold nanoparticles with a citrate capping with different sizes, before and after calorimetry.

As for "PEGylated" nanoparticles, the results show that there are no changes in the spectra (**Figure 39**). Two possible explanations can be given. One hand, that there are no changes in the structure of the particles. On the other hand, it can be said that the energy that the sample absorbed was higher than the pseudo-covalent bond that binds the thiolated molecules to the gold surface (≃ 45 kcal/mol) [26]. Further on, it will be calculated the energy that each sample absorbs, so it will be possible to state which hypothesis is more accurate.

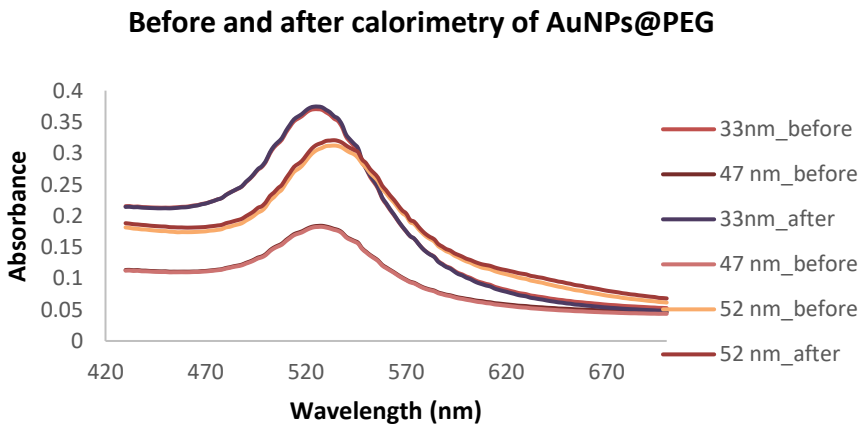

Figure 39: Absorbance spectra of "PEGylated" gold nanoparticles with different sizes, before and after calorimetry.

3.7. Elimination of polidispersivity

Different variations of the method described above were attempted. Initially it was tested in a Falcon tube, then it was tested in a centrifuge tube. The volume of particles, the volume of each layer of sucrose, the centrifugation velocity suffered variations. The protocol above is the result of these tests.

The following figures (**Figures 40** and **41**) illustrate the results. Bear in mind that tube was divided in 4 layers (named F1, F2, F3 and F4) for a better understanding of the migration of the AuNPs. As it is perceived, in both figures some particles migrated more than others. It is expected that the bigger they are, the farther they migrate.

Firstly using gold nanoparticles with 15 nm in diameter (**Figure 40**), after centrifugation they remain in the F1 area, this corresponds to the phase where particles with a size between 10 and 20 nm remain.

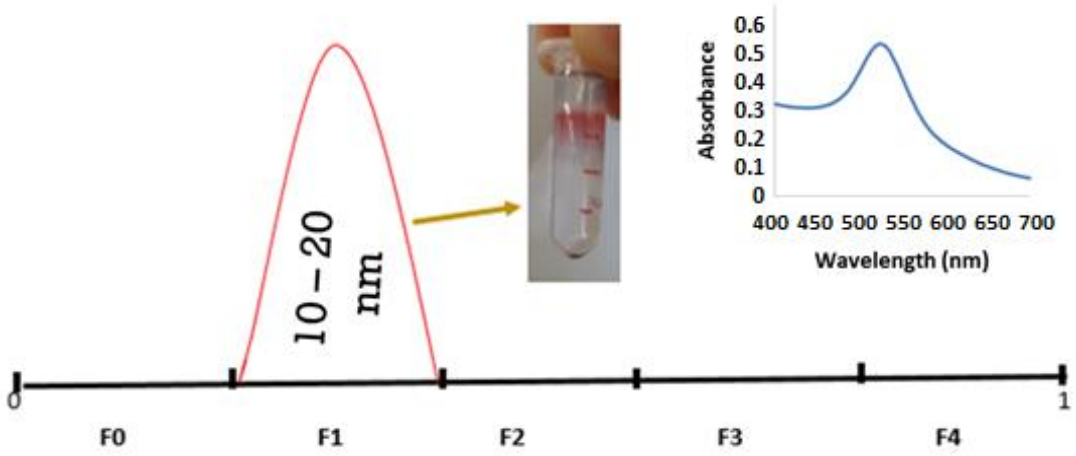

Figure 40: Size separation of citrate capping gold nanoparticles (15 nm) through centrifugation.

By using AuNPs with 35 nm in diameter (**Figure 41**), the after centrifugation lead them to migrate to the F2 area, where particles with a diameter between 25 and 40 nm remain.

Comparing in both situations, spectra of before and after this method was applied, it is possible to perceive a narrowing in the SPR band (**Table 3.2**).

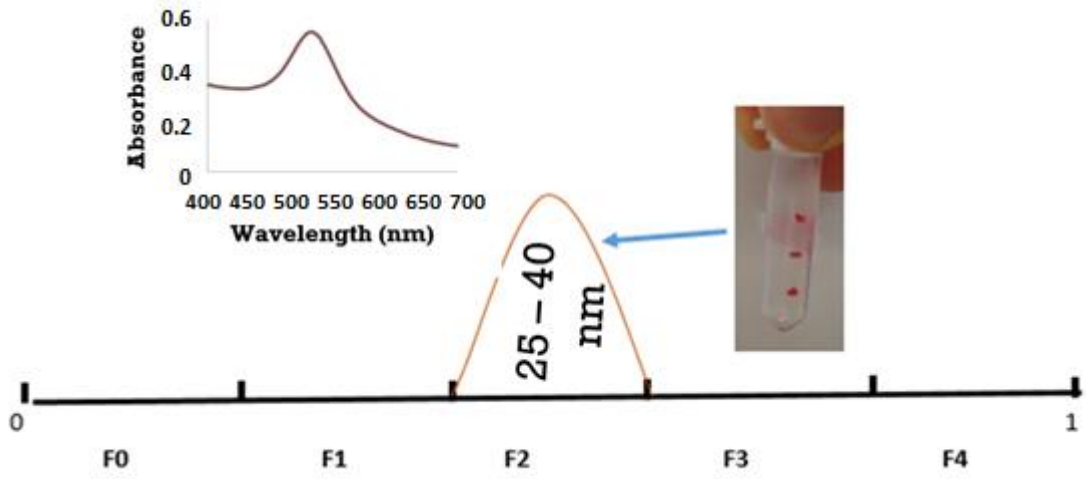

Figure 41: Size separation of citrate capping gold nanoparticles (35 nm) through centrifugation.

Table 3.2: Difference in half-width before and after centrifugation, using 2 different sizes of AuNPs.

Identification	Half-width before centrifugation (nm)	Half-width after centrifugation (nm)
AuNPs@Citrate (15 nm)	51	46
AuNPs@Cítrate (35 nm)	46	43

3.8. Density assessment

These measurements were done because there is no references in the literature related to the density of PBS, DMEM with phenol red and DMEM without phenol red.

It was expected that the densities were higher than water but not very different from it, and that was confirmed (**Table 3.3**).

Table 3.3: Density measurements using a tensiometer and pycnometer.

Material	ρ (Tensiometer) [kg/L]	ρ (Pycnometer) [kg/L]
PBS	1.0031	1.0060 ± 0.0006
DMEM (phenol red)	1.0052	1.0076 ± 0.0004
DMEM	1.0072	1.0079 ± 0.0005

3.9. Differential scanning calorimetry analysis

Differential scanning calorimetry (DSC) is a thermoanalytical technique that analyses that measures the difference in the amount of heat that it is used to raise the temperature of a sample and a reference. Normally it is used to analyze the phase shift in different materials [60]. The purpose of using this technique in the context of this work is to know the specific heat of PBS, DMEM (with phenol red) and DMEM (without phenol red).

The DSC results (**Appendix C**) presents graphics of heat flow as a function of temperature. The specific heat is the tangent in a specific point (**Figure 42**) and it is measured to each temperature. A higher specific heat means that is needed more energy to raise 1º C of temperature per gram of sample.

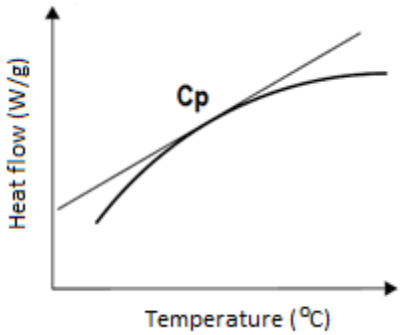

Figure 42: Graphic elucidation of how to calculate specific heat.

Analyzing the results (**Table 3.4**), comparing to the Cp of water (4.18 at 25 ºC) [61], the Cp of PBS revealed to be higher, this was expected because saline solutions normally require more time, higher energy to reach a specific temperature. As for the results DMEM with phenol red, it was expected that the DMEM with phenol red had an inferior Cp than the DMEM without phenol red because of the results of calorimetry in the control of the two media. In the following section, it will be given an explanation for why this happens.

Table 3.4: Specific heat measurements using differential scanning calorimetry,

Material	Cp (J/g.K)
PBS	4.278 ± 0.180 (25 ºC)
DMEM (phenol red)	3.994 ± 0.230 (25 ºC)
DMEM	3.918 ± 0.200 (25 ºC)

3.10. Photothermal yield

After all the experiments of calorimetry to know which particles heat more, to know which particles have a higher photothermal conversion capacity, it is important to know what is the photothermal yield of each experiment, in order to have a better comprehension of how much energy is converted to heat, and how much it is dispersed to the environment. To calculate the Photothermal yield, it is indispensable to know how much photons are absorbed by each sample, and this is done by means of Actinometry assays; and the heat transfer (**Appendix D**).

Before presenting the results, the variables that can affect the yield of an experiment are as following:

- Concentration of the sample;
- Absorbance/scattering capacity of the sample (that is related too with the previous point);
- Density;
- Specific heat;
- Difference of temperatures (ΔΔT).

Looking at previous results, due to the fact the density is very similar in the difference media, as well as the specific heat, the variables that will affect mostly the outcome are: the concentration, the absorbance/capacity of the sample (that is mainly media) and the difference of temperatures in the experiments.

Figure 3.5: Photothermal yield summary.

			Yield (%)			
Medium	**Conditions**	**Laser Mode**	**15 nm**	**33 nm**	**47 nm**	**53 nm**
Water	*AuNPs@Citrate (1 nM)*	*CW*	-	47.03	27.02	33.84
	AuNPs@PEG (1 nM)	*CW*	-	66.78	65.24	64.87
PBS	*AuNPs@Citrate (1 nM)*	*CW*	-	97.16	85.29	94.79
	AuNPs@PEG (1 nM)	*CW*	-	136.11	131.34	124.06
DMEM (with phenol red)	*AuNPs@Citrate (10 nM)*	*CW*	0.00	11.32	-	0.00
	AuNPs@PEG (10 nM)	*CW*	0.00	1.5	-	5.17
	AuNPs@Citrate (10 nM)	Pulsed	0.00	45.27	-	32.58
	AuNPs@PEG (10 nM)	Pulsed	7.00	4.67	-	2.83
DMEM (without phenol red)	*AuNPs@Citrate (10 nM)*	*CW*	28.80	19.84	-	-
	AuNPs@PEG (10 nM)	*CW*	16.82	12.37	-	-
	AuNPs@Citrate (10 nM)	Pulsed	22.25	15.01	-	-
	AuNPs@PEG (10 nM)	Pulsed	24.82	18.79	-	-
Egg white	*AuNPs@Citrate (10 nM)*	*CW*	28.80	19.84	-	-
	AuNPs@PEG (10 nM)	*CW*	37.57	24.61	-	-
	AuNPs@Citrate (10 nM)	Pulsed	16.82	12.37	-	-
	AuNPs@PEG (10 nM)	Pulsed	33.82	32.64	-	-

Analyzing **table 3.5**, it is safe to say that the results of the photothermal yield are coherent to what was expected accordingly with the calorimetry results. As for the PBS, the results do not make sense. It was expected that the yield would be lower due to the fact that nanoparticles aggregate, thus increasing the scattering component dramatically, which does not contribute to the elevation of temperature. The results of the photothermal yield in DMEM with phenol red were somehow expected. As it was stated earlier, the concentration, the absorbing/scattering capacity of the samples and the temperature variation are the variables that would affect the most the results. Going back to **subsection 3.6.1.** it is visible that the calorimetry results are not coherent, largely to the fact that the phenol red in DMEM, absorbs a considerable amount of energy, that is why pulsed mode is used in attempt of minimizing that absorption.

3.11. Cell assays

Using HCT116 cell lines, it was done an assay in order to compare 15 nm AuNPs with a capping of citrate and a capping of polyethylene glycol. Firstly, doing the calorimetry, but with a different step than previous experiments. In this part, first the

particles are incubated for 2 hours, the media is exchanged, and then it is done the calorimetry.

Normalizing the graphic in order to see the real difference between the AuNPs, there is no evident difference between them (**Figure 43**).

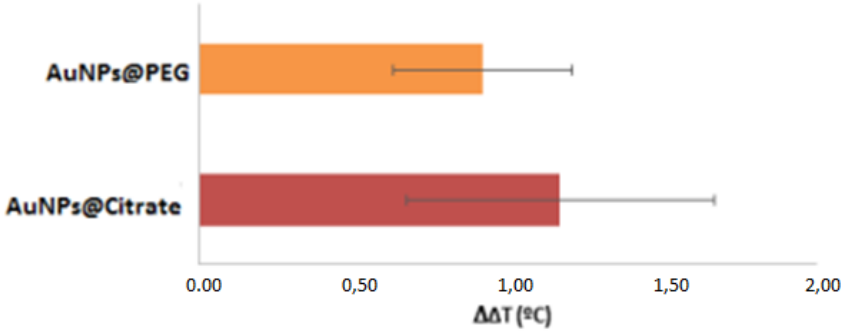

Figure 43: Comparing results of calorimetry with 15 nm citrate capping and "PEGylated" gold nanoparticles in HCT116 cells.

Looking to the MTS results (**Figure 44**), the value superior to 100 % is due to differences in metabolism of cells and interferences with the MTS. Pegylated nanoparticles show a (little) difference in viability as comparison with citrate capped AuNPs. This corroborates previous results in calorimetry. The photothermal conversion capacities using AuNPs@PEG was almost higher than in AuNPs@Citrate in most experiments.

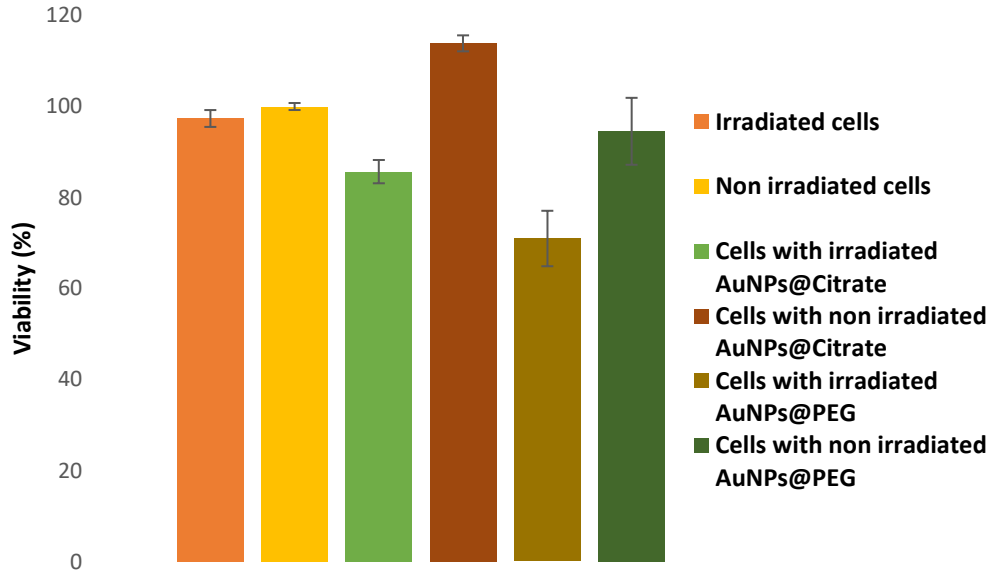

Figure 44: MTS results of assay with 15 nm citrate capping and "PEGylated" gold nanoparticles in HCT116 cells.

4. CONCLUSIONS AND FUTURE WORK

Cancer is the second leading cause of mortality throughout the world. Finding a way to turn this terrible disease into a chronic illness still remains a challenge. The major obstacle with conventional methods is still the lack of selectivity and specificity. Due to this issue, alternative therapies have been tested that can be used alone or concomitantly with others. Photothermal therapy has shown great promise to achieve the goal. Using nanotechnology to work as coadjutant is being applied in medicine's field towards improving cell tumor target and reducing the damages of healthy cells.

The present work addressed the photothermal characterization of AuNPs with different sizes with the perspective of doing photothermal ablation of cancer cells, in the future.

Different synthesis of AuNPs@Citrate were successfully done, with good reproducibility. However, synthesis control of spherical and monodisperse is not straightforward. To improve this, another reactant needs to be added to the reaction. Using tannic acid or another reduction agent (e.g. hydroquinone) can solve this issue [62-64].

Gold nanoparticles were successfully functionalized with PEG in order to increase their stability and biocompatibility. It was concluded that AuNPs@Citrate and AuNPs@PEG synthesized via this seeding method are not stable in PBS.

The Ellman's assay was used to assess its effectiveness. It was stated above that the results of this test are subjected with different interferences. Using ^{1}H NMR with the following protocol (**Appendix E**) can surpass that problem, thus achieving a better perception of nanoparticle functionalization effectiveness.

Calorimetry studies in different media were done. According to the results it was concluded that the photothermal conversion capability is higher in small AuNPs, almost saying that the photothermal conversion capacity and size are inversely proportional. Furthermore, AuNPs@PEG are more efficient in converting light to heat than AuNPs@Citrate.

The main adversity throughout this thesis was the molar extinction coefficient calculation for different particles, which allows you to know the precise concentration of each batch of nanoparticles. This was mainly due to the fact that each solution presented great heterogeneity of sizes. Hence, it was tried a normalization of the absorbance of each of them to try to make comparisons. In order to avoid problems with future synthesis (and

characterization) of gold nanoparticles with different sizes, the idea of creating an algorithm to calculate molar extinction coefficient with great accuracy has emerged, and a program in Python is being developed for that end.

This thesis is not an end, it is a path (one of many) that was followed. In order to perceive how things could be done in the right way, mistakes have to be made, and that is how we evolve not only as scientists but also as human beings.

5. REFERENCES

[1] McGuire, S. (2016). World cancer report 2014. Geneva, Switzerland: World Health Organization, international agency for research on cancer, WHO Press, 2015. *Advances in Nutrition: An International Review Journal*, *7*(2), 418-419.

[2] Siegel, R. L., Miller, K. D., Jemal, A. (2016). Cancer statistics, 2016. *CA: a cancer journal for clinicians*, *66*(1), 7-30.

[3] Conde, J. (2015). The Golden Age in Cancer Nanobiotechnology: Quo Vadis?. *Frontiers in bioengineering and biotechnology*, *3*.

[4] Fitzmaurice, C., Allen, C., Barber, R. M., Barregard, L., Bhutta, Z. A., Brenner, H Dicker, D.J., Chimed-Orchir, O., Dandona, R., Dandona, L., Fleming, T., Forouzanfar, M. H., Hancock, J., Hay, R. J., Hunter-Merrill, R., Huynh, C., Hosgood, H. D., Johnson, C. O., Jonas, J. B., Khubchandani, J., Kumar, G. A., Kutz, M., Lan, Q., Larson, H. J., Liang, X., Lim, S. S., Lopez, A. D., MacIntyre, M. F., Marczak, L., Marquez, N., Mokdad, A. H., Pinho, C., Pourmalek, F., Salomon, J. A., Sanabria, J. R., Sandar, L., Sartorius, B., Schwartz, S. M., Shackelford, K. A., Shibuya, K., Stanaway, J., Steiner, C., Sun, J., Takahashi, K., Vollset, S. E., Vos, T., Wagner, J. A., Wang, H., Westerman, R., Zeeb, H., Zoeckler, L., Abd-Allah, F., Ahmed, M. B., Alabed, S., Alam, N. K., Aldhahri, S. F., Alem, G., Alemayohu, M. A., Ali, R., Al-Raddadi, R., Amare, A., Amoako, Y., Artaman, A., Asayesh, H., Atnafu, N., Awasthi, A., Saleem, H. B., Barac, A., Bedi, N., Bensenor, I., Berhane, A., Bernabé, E., Betsu, B., Binagwaho, A., Boneya, D., Campos-Nonato, I., Castañeda-Orjuela, C., Catalá-López, F., Chiang, P., Chibueze, C., Chitheer, A., Choi, J. Y., Cowie, B., Damtew, S., das Neves, J., Dey, S., Dharmaratne, S., Dhillon, P., Ding, E., Driscoll, T., Ekwueme, D., Endries, A. Y., Farvid, M., Farzadfar, F., Fernandes, J., Fischer, F., G/Hiwot, T. T., Gebru, A., Gopalani, S., Hailu, A., Horino, M., Horita, N., Husseini, A., Huybrechts, I., Inoue, M., Islami, F., Jakovljevic, M., James, S., Javanbakht, M., Jee, S. H., Kasaeian, A., Kedir, M. S., Khader, Y. S., Khang, Y. H., Kim, D., Leigh, J., Linn, S., Lunevicius, R., El Razek, H. M. A., Malekzadeh, R., Malta, D. C., Marcenes, W., Markos, D., Melaku, Y. A., Meles, K. G., Mendoza, W., Mengiste, D. T., Meretoja, T. J., Miller, T. R., Mohammad, K. A., Mohammadi, A., Mohammed, S., Moradi-Lakeh, M., Nagel, G., Nand, D., Le Nguyen, Q., Nolte, S., Ogbo, F. A., Oladimeji, K. E., Oren, E., Pa, M., Park, E. K., Pereira, D. M., Plass, D., Qorbani, M., Radfar, A., Rafay, A., Rahman, M., Rana, S. M., Søreide, K., Satpathy, M., Sawhney, M., Sepanlou, S. G., Shaikh, M. A., She, J., Shiue, I., Shore, H. R., Shrime, M. G., So, S., Soneji, S., Stathopoulou, V., Stroumpoulis, K., Sufiyan, M. B., Sykes, B. L., Tabarés-Seisdedos, R., Tadese, F., Tedla, B. A., Tessema, G. A., Thakur, J. S., Tran, B. X., Ukwaja, K. N.,

Uzochukwu, B. S. C., Vlassov, V. V., Weiderpass, E., Wubshet Terefe, M., Yebyo, H. G., Yimam, H. H., Yonemoto, N., Younis, M. Z., Yu, C., Zaidi, Z., Zaki, M. E. S., Zenebe, Z. M., Murray, C. J. L., Naghavi, M. (2017). Global, regional, and national cancer incidence, mortality, years of life lost, years lived with disability, and disability-adjusted life-years for 32 cancer groups, 1990 to 2015: a systematic analysis for the global burden of disease study. *The Journal of the American Medical Association oncology*, *3*(4), 524-548.

[5] Van de Hulst, H. C. (1957). Light scattering by small particles. (Vol. 22). Courier Corporation.

[6] Faraday, M. (1996). Experimental relations of gold (and other metals) to light. *Society of Photo-Optical Instrumentation Engineers (SPIE) Milestone series ms*, *120*, 9-27.

[7] Bhattacharyya, D., Singh, S., Satnalika, N., Khandelwal, A., Jeon, S. H. (2009). Nanotechnology, big things from a tiny world: a review. *Nanotechnology*, *2*(3), 29-38.

[8] Eustis, S., El-Sayed, M. A. (2006). Why gold nanoparticles are more precious than pretty gold: noble metal surface plasmon resonance and its enhancement of the radiative and nonradiative properties of nanocrystals of different shapes. *Chemical society reviews*, *35*(3), 209-217.

[9] Reddy, V. R. (2006). Gold nanoparticles: synthesis and applications. *Synlett*, *2006*(11), 1791-1792.

[10] Parveen, S., Misra, R., Sahoo, S. K. (2012). Nanoparticles: a boon to drug delivery, therapeutics, diagnostics and imaging. *Nanomedicine: Nanotechnology, Biology and Medicine*, *8*(2), 147-166.

[11] Conde, J., Dias, J. T., Grazú, V., Moros, M., Baptista, P. V., de la Fuente, J. M. (2014). Revisiting 30 years of biofunctionalization and surface chemistry of inorganic nanoparticles for nanomedicine. *Frontiers in chemistry*, *2*.

[12] Kim, K. Y. (2007). Nanotechnology platforms and physiological challenges for cancer therapeutics. *Nanomedicine: Nanotechnology, Biology and Medicine*, *3*(2), 103-110.

[13] Heath, J. R., Davis, M. E. (2008). Nanotechnology and cancer. *Annual Review of Medicine*., *59*, 251-265.

[14] Sperling, R. A., Gil, P. R., Zhang, F., Zanella, M., Parak, W. J. (2008). Biological applications of gold nanoparticles. *Chemical Society Reviews*, *37*(9), 1896-1908.

[15] Salata, O. V. (2004). Applications of nanoparticles in biology and medicine. *Journal of nanobiotechnology*, *2*(1), 3.

[16] Pitkethly, M. J. (2004). Nanomaterials–the driving force. *Materials today*, *7*(12), 20-29.

[17] Mieszawska, A. J., Mulder, W. J., Fayad, Z. A., & Cormode, D. P. (2013). Multifunctional gold nanoparticles for diagnosis and therapy of disease. *Molecular pharmaceutics*, *10*(3), 831-847.

[18] Turkevich, J., Stevenson, P. C., Hillier, J. (1951). A study of the nucleation and growth processes in the synthesis of colloidal gold. *Discussions of the Faraday Society*, *11*, 55-75.

[19] Low, A., Bansal, V. (2010). A visual tutorial on the synthesis of gold nanoparticles. *Biomedical imaging and intervention journal*, *6*(1).

[20] Zhao, J., Friedrich, B. (2017). Synthesis of Gold Nanoparticles Via the Chemical Reduction Methods. Shaker.

[21] Huang, X., El-Sayed, M. A. (2011). Plasmonic photo-thermal therapy (PPTT). *Alexandria journal of medicine*, *47*(1), 1-9.

[22] Sun, Y., Xia, Y. (2002). Shape-controlled synthesis of gold and silver nanoparticles. *Science*, *298*(5601), 2176-2179.

[23] El-Brolossy, T. A., Abdallah, T., Mohamed, M. B., Abdallah, S., Easawi, K., Negm, S., Talaat, H. (2008). Shape and size dependence of the surface plasmon resonance of gold nanoparticles studied by Photoacoustic technique. *The European Physical Journal-Special Topics*, *153*(1), 361-364.

[24] Tiwari, P. M., Vig, K., Dennis, V. A., & Singh, S. R. (2011). Functionalized gold nanoparticles and their biomedical applications. *Nanomaterials*, *1*(1), 31-63.

[25] Thanh, N. T., Green, L. A. (2010). Functionalisation of nanoparticles for biomedical applications. *Nano Today*, *5*(3), 213-230.

[26] Bastús, N. G., Comenge, J., & Puntes, V. (2011). Kinetically controlled seeded growth synthesis of citrate-stabilized gold nanoparticles of up to 200 nm: size focusing versus Ostwald ripening. *Langmuir*, *27*(17), 11098-11105.

[27] Love, J. C., Estroff, L. A., Kriebel, J. K., Nuzzo, R. G., & Whitesides, G. M. (2005). Self-assembled monolayers of thiolates on metals as a form of nanotechnology. *Chemical reviews*, *105*(4), 1103-1170.

[28] Doria, G., Conde, J., Veigas, B., Giestas, L., Almeida, C., Assunção, M., Rosa, P., Baptista, P. V. (2012). Noble metal nanoparticles for biosensing applications. *Sensors*, *12*(2), 1657-1687.

[29] Manson, J., Kumar, D., Meenan, B. J., Dixon, D. (2011). Polyethylene glycol functionalized gold nanoparticles: the influence of capping density on stability in various media. *Gold bulletin*, *44*(2), 99-105.

[30] Jokerst, J. V., Lobovkina, T., Zare, R. N., Gambhir, S. S. (2011). Nanoparticle PEGylation for imaging and therapy. *Nanomedicine*, *6*(4), 715-728.

[31] Huang, X., Jain, P. K., El-Sayed, I. H., El-Sayed, M. A. (2008). Plasmonic photothermal therapy (PPTT) using gold nanoparticles. *Lasers in medical science*, *23*(3), 217.

[32] Cordeiro, M., Ferreira Carlos, F., Pedrosa, P., Lopez, A., Baptista, P. V. (2016). Gold Nanoparticles for Diagnostics: *Advances towards Points of Care*. Diagnostics, 6(4), 43.

[33] Abadeer, N. S., Murphy, C. J. (2016). Recent progress in cancer thermal therapy using gold nanoparticles. *The Journal of Physical Chemistry C*, *120*(9), 4691-4716.

[34] Huang, X., El-Sayed, M. A. (2010). Gold nanoparticles: optical properties and implementations in cancer diagnosis and photothermal therapy. *Journal of advanced research*, *1*(1), 13-28.

[35] Wittstock, A., Biener, J., Bauemer, M. (2012). Nanoporous gold: from an ancient technology to a high-tech material (Vol. 22). Royal Society of Chemistry.

[36] Larguinho, M., Canto, R., Cordeiro, M., Pedrosa, P., Fortuna, A., Vinhas, R., & Baptista, P. V. (2015). Gold nanoprobe-based non-crosslinking hybridization for molecular diagnostics. *Expert review of molecular diagnostics*, *15*(10), 1355-1368.

[37] Baptista, P., Pereira, E., Eaton, P., Doria, G., Miranda, A., Gomes, I., Quaresma, P., Franco, R. (2008). Gold nanoparticles for the development of clinical diagnosis methods. *Analytical and bioanalytical chemistry*, *391*(3), 943-950.

[38] Baños, D., Collado-González, M., Espín, V. F., Montalbán, M. G., Pamies, R., Cifre, J. G. H., Guillermo, F. (2015). Aggregation behaviour of gold nanoparticles in presence of chitosan. *Journal of Nanoparticle Research*, *17*, 1-10.

[39] Baskar, R., Lee, K. A., Yeo, R., Yeoh, K. W. (2012). Cancer and radiation therapy: current advances and future directions. *International journal of medical sciences*, *9*(3), 193.

[40] Sutradhar, K. B., Amin, M. L. (2014). Nanotechnology in cancer drug delivery and selective targeting. *International Scholarly Research Notices: Nanotechnology*, *2014*.

[41] Yao, C., Zhang, L., Wang, J., He, Y., Xin, J., Wang, S., Xu, H., Zhang, Z. (2016). Gold nanoparticle mediated phototherapy for cancer. *Journal of Nanomaterials*, *2016*.

[42] Jiang, K., Smith, D. A., Pinchuk, A. (2013). Size-dependent photothermal conversion efficiencies of plasmonically heated gold nanoparticles. *The Journal of Physical Chemistry C*, *117*(51), 27073-27080.

[43] Elbialy, N., Abdelhamid, M., Youssef, T. (2010). Low power argon laser-induced thermal therapy for subcutaneous Ehrlich carcinoma in mice using spherical gold nanoparticles. *Journal of biomedical nanotechnology*, *6*(6), 687-693.

[44] Haiss, W., Thanh, N. T., Aveyard, J., Fernig, D. G. (2007). Determination of size and concentration of gold nanoparticles from UV-vis spectra. *Analytical chemistry*, *79*(11), 4215-4221.

[45] Conde, J., Rosa, J., Baptista, P. (2013). Gold-nanobeacons as a theranostic system for the detection and inhibition of specific genes. *Protocol Exchange*, *10*.

[46] Chen, W., Zhao, Y., Seefeldt, T., Guan, X. (2008). Determination of thiols and disulfides via HPLC quantification of 5-thio-2-nitrobenzoic acid. *Journal of pharmaceutical and biomedical analysis*, *48*(5), 1375-1380.

[47] Aitken, A., Learmonth, M. (2002). Estimation of disulfide bonds using Ellman's reagent. *The Protein Protocols Handbook*, 595-596.

[48] Minai, L., Yeheskely-Hayon, D., Yelin, D. (2013). High levels of reactive oxygen species in gold nanoparticle-targeted cancer cells following femtosecond pulse irradiation. *Scientific reports*, *3*.

[49] Malich, G., Markovic, B., Winder, C. (1997). The sensitivity and specificity of the MTS tetrazolium assay for detecting the in vitro cytotoxicity of 20 chemicals using human cell lines. *Toxicology*, *124*(3), 179-192.´

[50] Wu, W., Huang, J., Wu, L., Sun, D., Lin, L., Zhou, Y., Wang, H., Li, Q. (2013). Two-step size-and shape-separation of biosynthesized gold nanoparticles. *Separation and Purification Technology*, *106*, 117-122.

[51] Kumar, S. A., Peter, Y. A., Nadeau, J. L. (2008). Facile biosynthesis, separation and conjugation of gold nanoparticles to doxorubicin. *Nanotechnology*, *19*(49), 495101.

[52] Liu, X., Atwater, M., Wang, J., Huo, Q. (2007). Extinction coefficient of gold nanoparticles with different sizes and different capping ligands. *Colloids and Surfaces B: Biointerfaces*, *58*(1), 3-7.

[53] Baptista, P., Doria, G., Henriques, D., Pereira, E., Franco, R. (2005). Colorimetric detection of eukaryotic gene expression with DNA-derivatized gold nanoparticles. *Journal of biotechnology*, *119*(2), 111-117.

[54] Bogatyrev, V. A., Dykman, L. A., Khlebtsov, B. N., Khlebtsov, N. G. (2004). Measurement of mean size and evaluation of polydispersity of gold nanoparticles from spectra of optical absorption and scattering. *Optics and Spectroscopy*, *96*(1), 128-135.

[55] Khlebtsov, B. N., Khlebtsov, N. G. (2011). On the measurement of gold nanoparticle sizes by the dynamic light scattering method. *Colloid Journal*, *73*(1), 118-127.

[56] Reimer, L. (2013). Transmission electron microscopy: physics of image formation and microanalysis (Vol. 36). Springer.

[57] Capek, I. (2017). Noble Metal Nanoparticles: Preparation, Composite Nanostructures, Biodecoration and Collective Properties. Springer.

[58] Anderson, A. C., Wolfe, J. P. (Eds.). (2012). Phonon Scattering in Condensed Matter V: Proceedings of the Fifth International Conference Urbana, Illinois, June 2–6, 1986 (Vol. 68). Springer Science & Business Media.

[59] Chen, H., Shao, L., Ming, T., Sun, Z., Zhao, C., Yang, B., Wang, J. (2010). Understanding the photothermal conversion efficiency of gold nanocrystals. *Small*, *6*(20), 2272-2280.

[60] Höhne, G., Hemminger, W. F., Flammersheim, H. J. (2013). *Differential scanning calorimetry*. Springer Science & Business Media.

[61] Osborne, N. S., Stimson, H. F., Ginnings, D. C. (1939). *Measurements of Heat Capacity and Heat of Vaporization of Water in the Range of 0° to 100° C*. US Department of Commerce, National Bureau of Standards.

[62] Jana, N. R., Gearheart, L., Murphy, C. J. (2001). Seeding growth for size control of 5− 40 nm diameter gold nanoparticles. *Langmuir*, *17*(22), 6782-6786.

[63] Perrault, S. D., & Chan, W. C. (2009). Synthesis and surface modification of highly monodispersed, spherical gold nanoparticles of 50− 200 nm. *Journal of the American Chemical Society*, *131*(47), 17042-17043.

[64] Senoudi, A. R., Chabane Sari, S. M., Hakem, I. F. (2014). Analysis of the evolution of tannic acid stabilized gold nanoparticles using mie theory. *International journal of analytical chemistry*, *2014*.

[65] Smith, A. M., Marbella, L. E., Johnston, K. A., Hartmann, M. J., Crawford, S. E., Kozycz, L. M., Seferes,, D. S., Millstone, J. E. (2015). Quantitative analysis of thiolated ligand exchange on gold nanoparticles monitored by 1H NMR spectroscopy. *Analytical Chem*istry *87*(5), 2771-2778.

[66] Bharti, S. K., Roy, R. (2012). Quantitative 1 H NMR spectroscopy. *TrAC Trends in Analytical Chemistry*, *35*, 5-26.

[67] Alvarado, E. (2010). Practical guide for quantitative 1D NMR integration. University of Michigan.

6. APPENDICES

6.1. Appendix A

d/ nm	ε_{450} / $M^{-1}cm^{-1}$	d/ nm	ε_{450} / $M^{-1}cm^{-1}$	d/ nm	ε_{450} / $M^{-1}cm^{-1}$
2	4.25E+05	35	3.21E+09	68	2.50E+10
3	1.49E+06	36	3.52E+09	69	2.61E+10
4	3.62E+06	37	3.84E+09	70	2.71E+10
5	7.20E+06	38	4.18E+09	71	2.82E+10
6	1.26E+07	39	4.54E+09	72	2.93E+10
7	2.03E+07	40	4.92E+09	73	3.05E+10
8	3.07E+07	41	5.32E+09	74	3.16E+10
9	4.43E+07	42	5.74E+09	75	3.28E+10
10	6.15E+07	43	6.18E+09	76	3.40E+10
11	8.27E+07	44	6.65E+09	77	3.52E+10
12	1.09E+08	45	7.13E+09	78	3.64E+10
13	1.39E+08	46	7.65E+09	79	3.77E+10
14	1.76E+08	47	8.18E+09	80	3.89E+10
15	2.18E+08	48	8.74E+09	81	4.02E+10
16	2.67E+08	49	9.32E+09	82	4.14E+10
17	3.24E+08	50	9.92E+09	83	4.27E+10
18	3.87E+08	51	1.06E+10	84	4.40E+10
19	4.60E+08	52	1.12E+10	85	4.53E+10
20	5.41E+08	53	1.19E+10	86	4.65E+10
21	6.31E+08	54	1.26E+10	87	4.78E+10
22	7.31E+08	55	1.33E+10	88	4.91E+10
23	8.42E+08	56	1.41E+10	89	5.04E+10
24	9.64E+08	57	1.48E+10	90	5.17E+10
25	1.10E+09	58	1.57E+10	91	5.30E+10
26	1.24E+09	59	1.65E+10	92	5.43E+10
27	1.40E+09	60	1.73E+10	93	5.56E+10
28	1.58E+09	61	1.82E+10	94	5.69E+10
29	1.76E+09	62	1.91E+10	95	5.82E+10
30	1.96E+09	63	2.00E+10	96	5.94E+10
31	2.18E+09	64	2.10E+10	97	6.07E+10
32	2.41E+09	65	2.19E+10	98	6.19E+10
33	2.66E+09	66	2.29E+10	99	6.31E+10
34	2.93E+09	67	2.40E+10	100	6.44E+10

Figure 45: Molar extinction coefficient for the diameters of the gold nanoparticles [44].

6.2. Appendix B

Sample measurement with Dynamic Light Scattering

This protocol was done with the purpose of helping who is having (serious) difficulties with DLS, both for the appearance of exclamation marks and for measurements in which the presented values of average hydrodynamic diameter and polydispersity index are not being minimally reproducible.

Note: The original protocol is in Portuguese in order to assist full comprehension by the students of different levels (undergraduate, master, and others).

Next, there are presented the parameters that I use when I am not being able to get results by the usual way (and the reason why I use them):

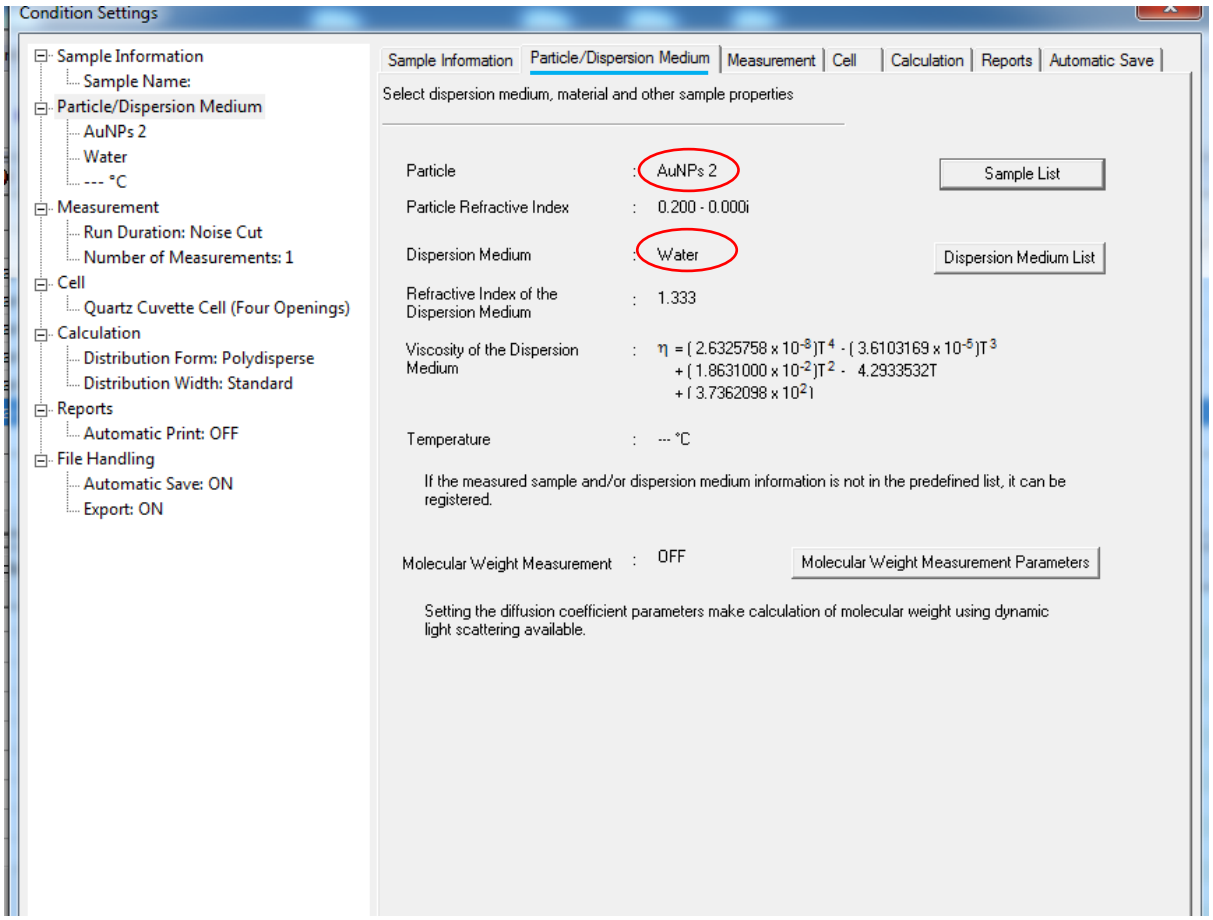

Figure 46: SZ-100 Horiba software – Condition Settings: Particle/Dispersion Medium window.

The medium varies from person to person (different samples), normally ***water*** is used as dispersion medium. Regarding the particles, before I used mono-polystyrene because I was taught that their refractive index was close to that of gold. According to a

constant table, the refractive index of gold is about 0.27732, while that of the mono-polystyrene is 1.5916. I think it is more correct to use the first, so when I choose the type of sample in the software I choose the ***AuNPs2 option***.

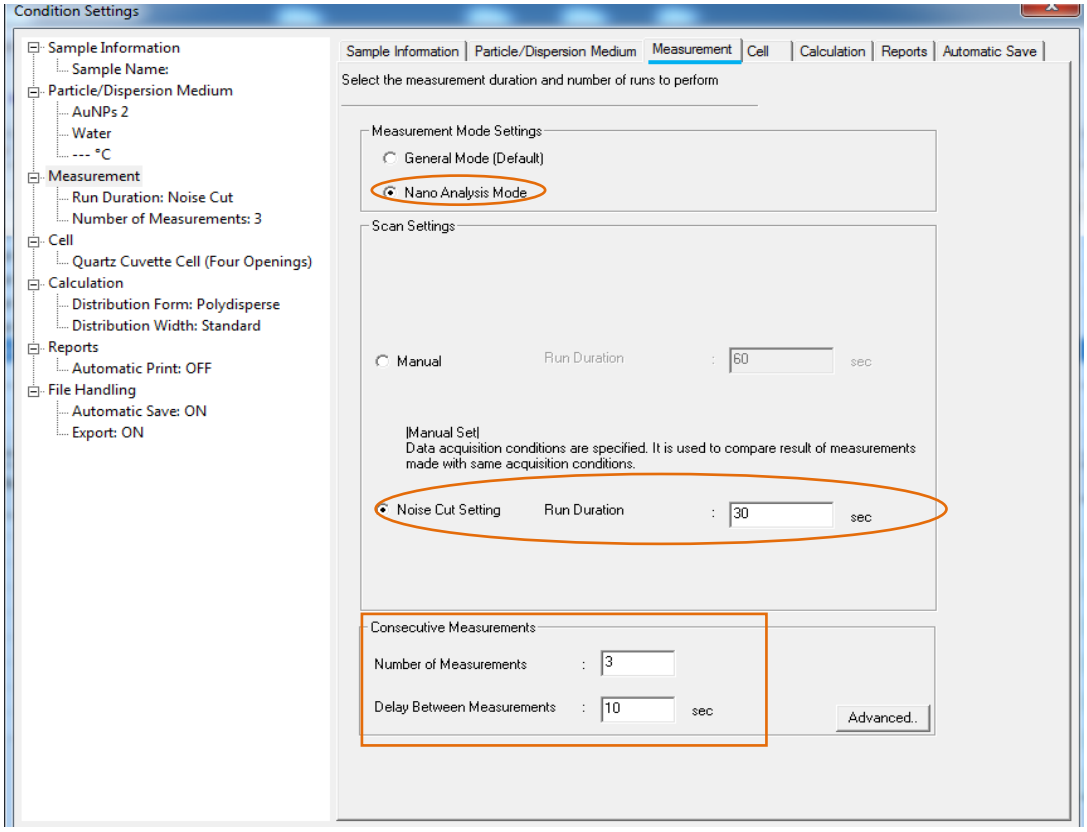

Figure 47: SZ-100 Horiba software – Condition Settings: Measurement window.

According to Horiba, the *Nano Analysis Mode* is used for when you have samples with particles of size closer to the lower limit of the apparatus's LOQ. When using this mode, it takes a lot more time to do the analysis because it is does a calibration / optimization to several parameters before carrying out the measurement itself.

I also use the noise cut tool between 30 to 60 seconds. What happens when using this technique is that when measuring, the autocorrelation curve undergoes less variations, it gives idea that there is a "slowing down" of the measurement, that it is done more slowly.

As for the number of measurements I always do 3, and the delay between them always custom it between 10 and 20 seconds. There is no rational explanation for this last parameter, it is just empirical, I have used it with delay and without it, and I get better results using it this way.

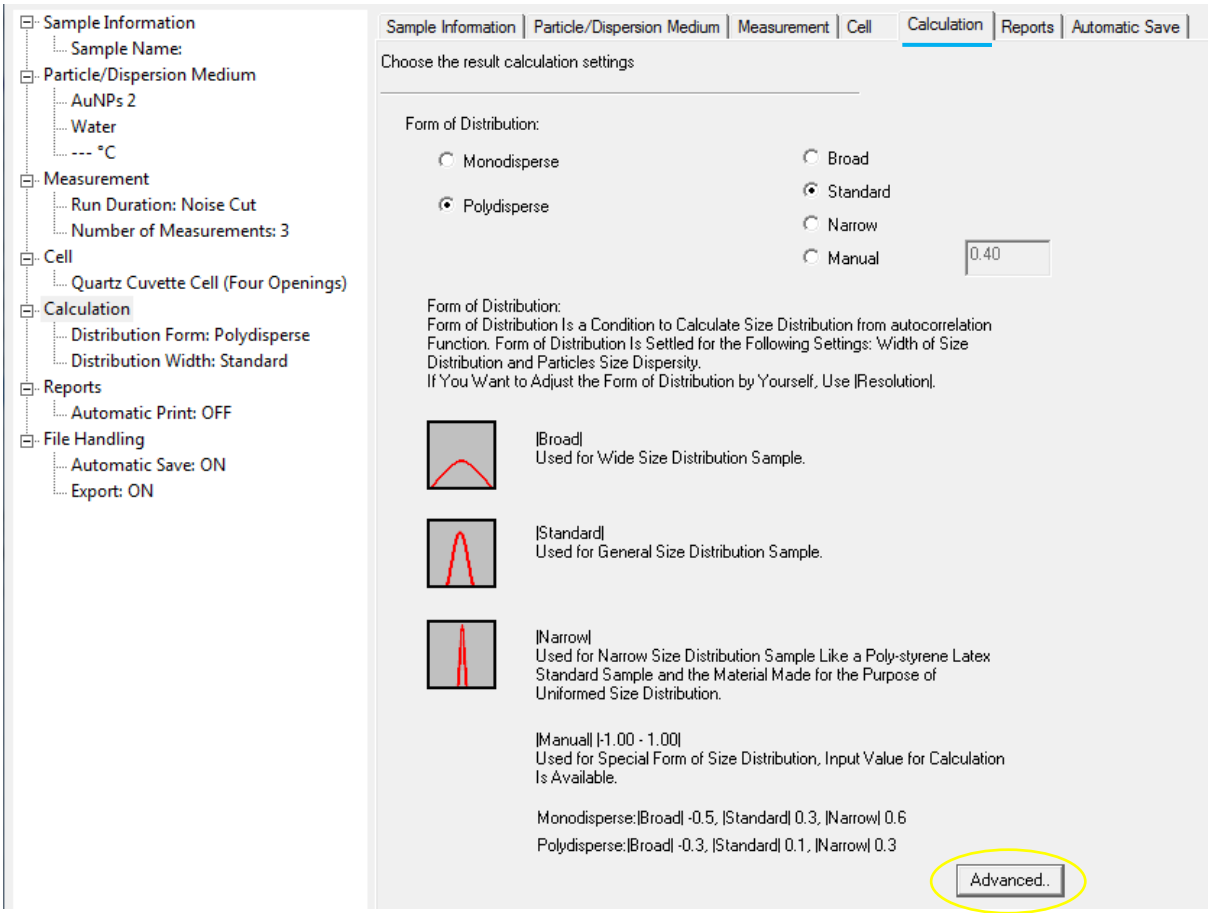

Figure 48: SZ-100 Horiba software – Condition Settings: Calculation window.

When my sample is 15 nm AuNPs@Citrate I assume that my sample is monodisperse. In all other situations, I always choose the standard polydispersed distribution parameter. Hitting the button *Advanced*:

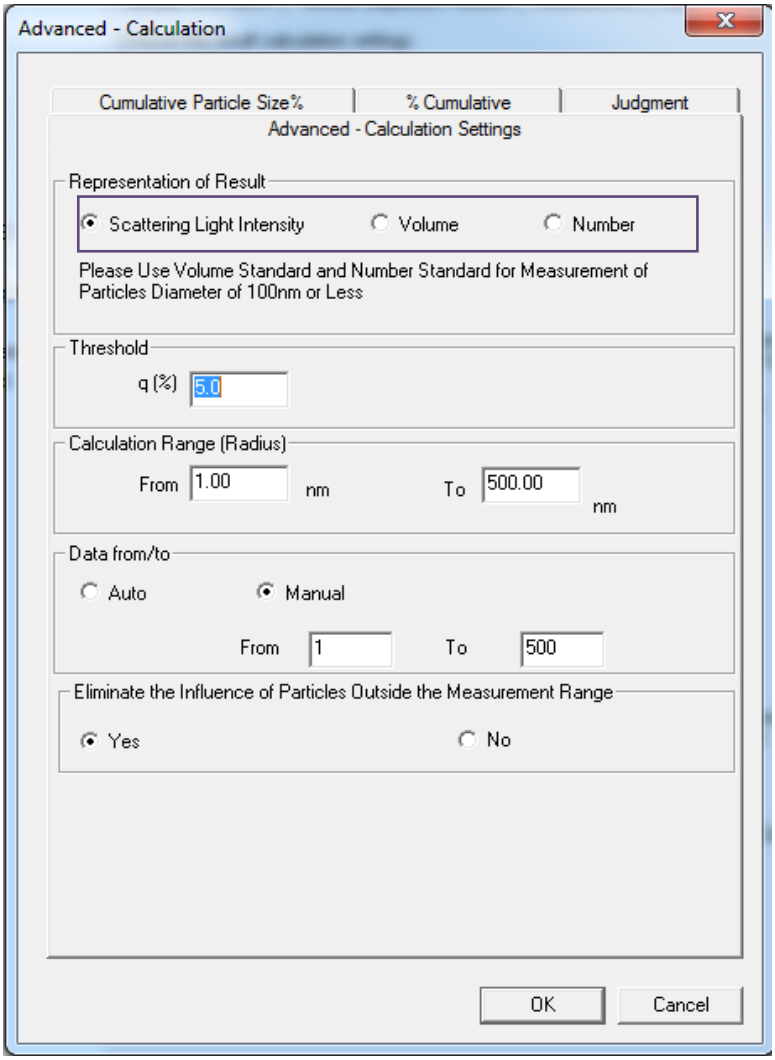

Figure 49: SZ-100 Horiba software – Condition Settings: Calculation, sub-window Advanced.

I use the representation of results as a function of ***Scattering Light Intensity***. This is because, when I used as a function of *the number of particles*, the software tends to reduce the polydispersity index to the maximum when the sample has a polydispersity index of more than 0.45, thus sacrificing the z-average value, leading to a misleading result.

Appendix C

PBS DSC results

(A)

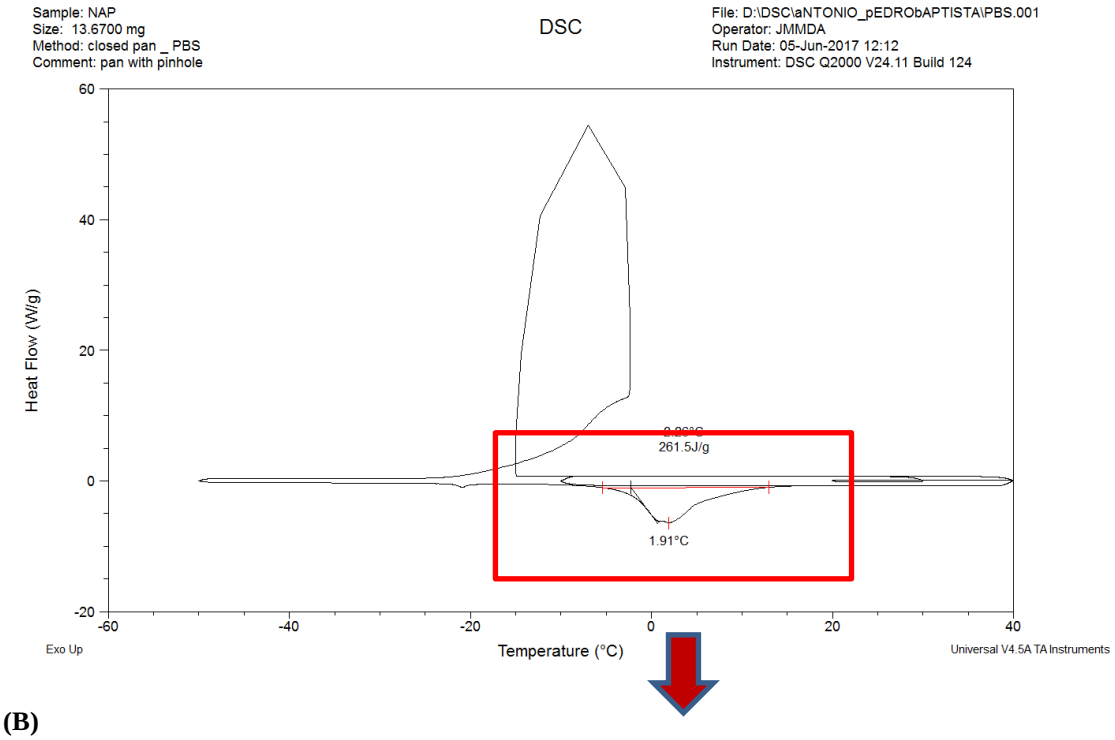

(B)

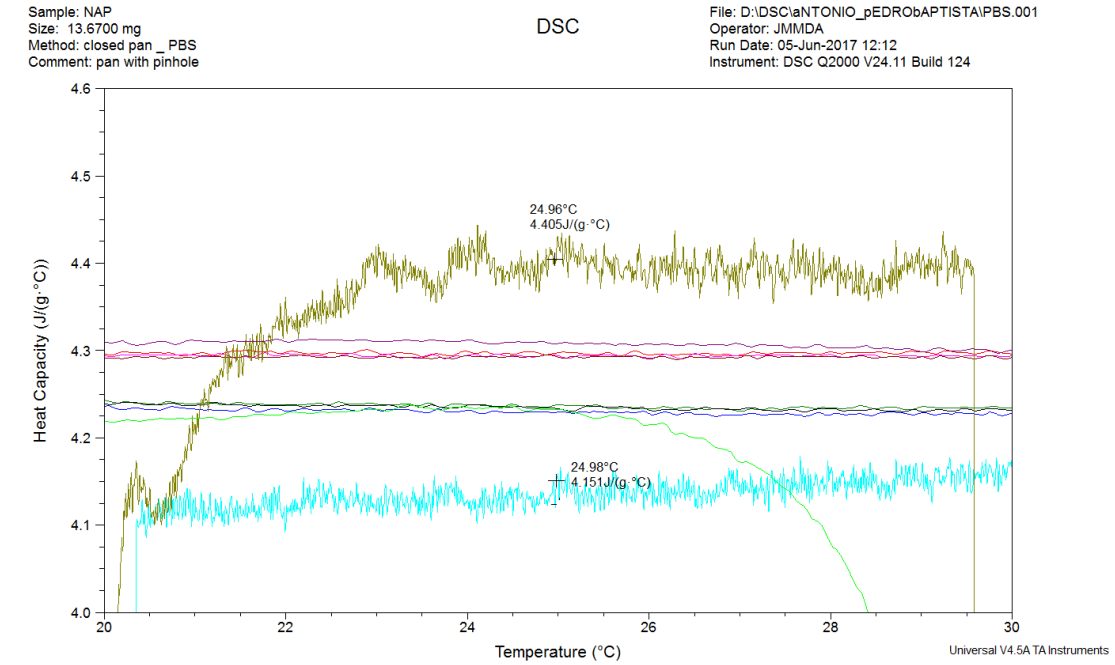

Figure 50: (A) Graphic of heat flow as a function of temperature in PBS. By doing the punctual tangent in the selected area, a graphic of specific heat as a function of temperature is obtained (B).

DMEM (with phenol red) DSC results

(A)

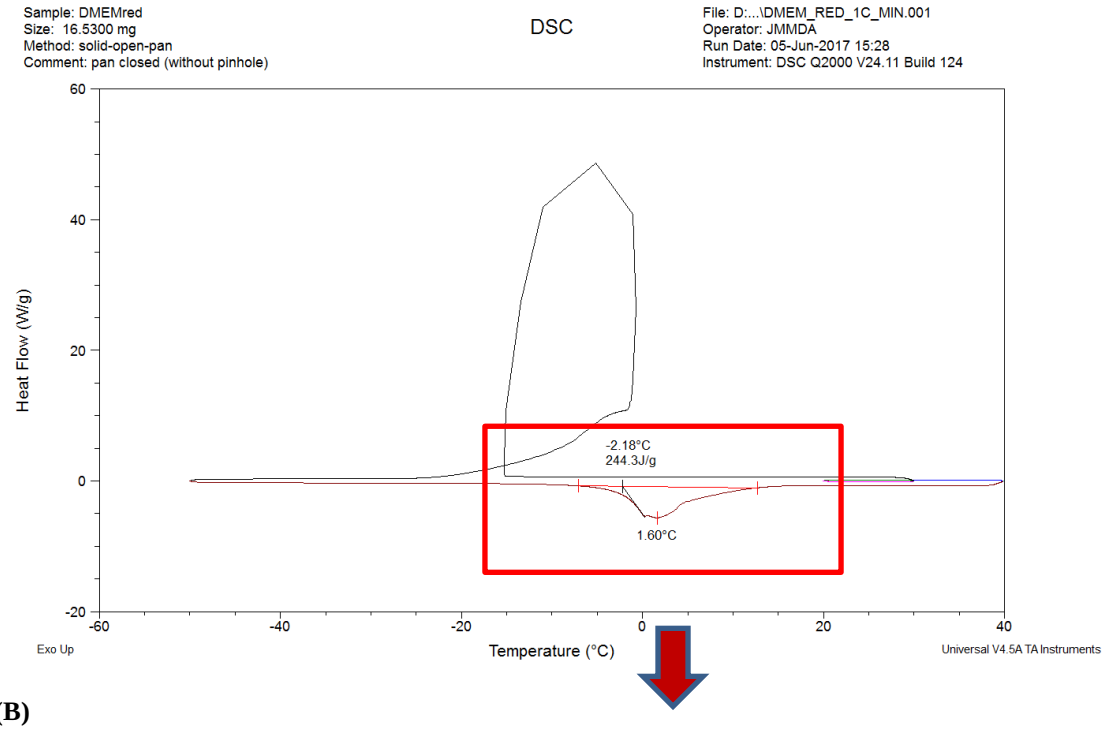

(B)

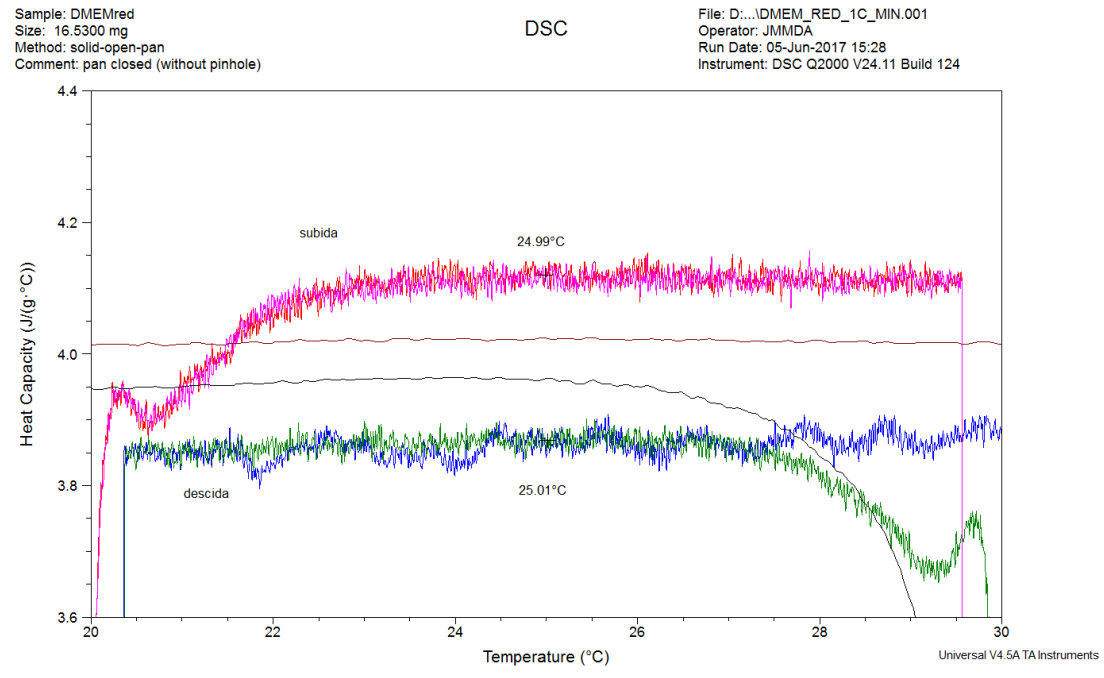

Figure 51: (A) Graphic of heat flow as a function of temperature in DMEM (with phenol red). By doing the punctual tangent in the selected area, a graphic of specific heat as a function of temperature is obtained (B).

DMEM (without phenol red) DSC results

(A)

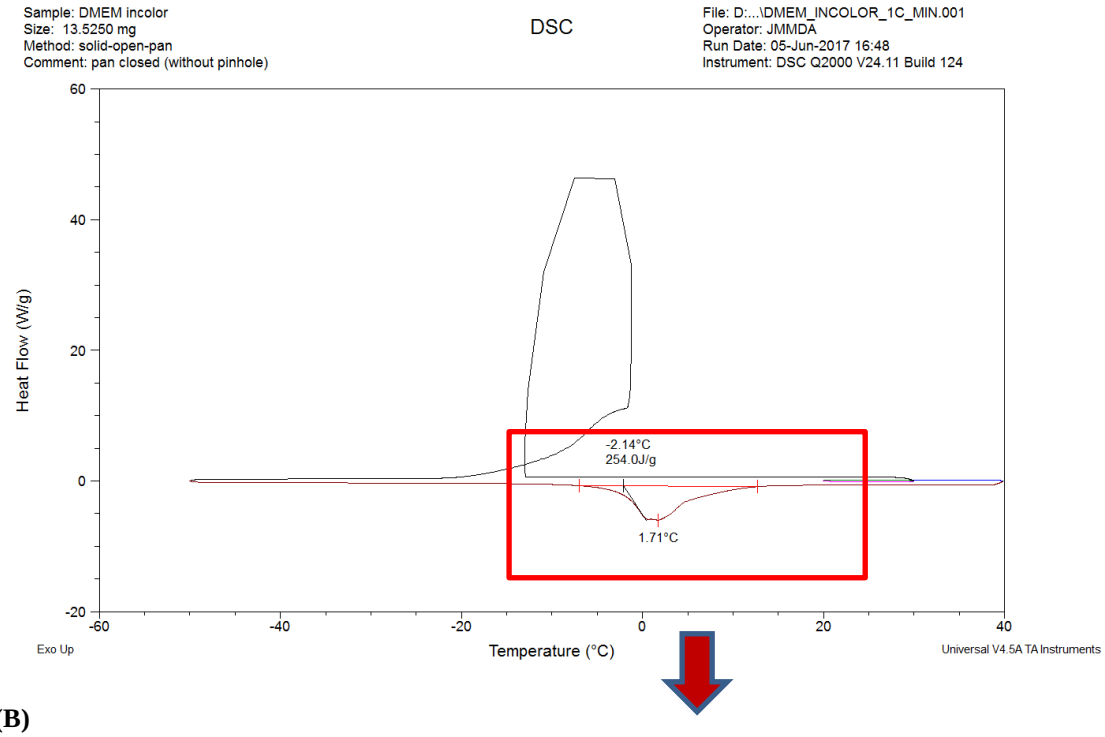

(B)

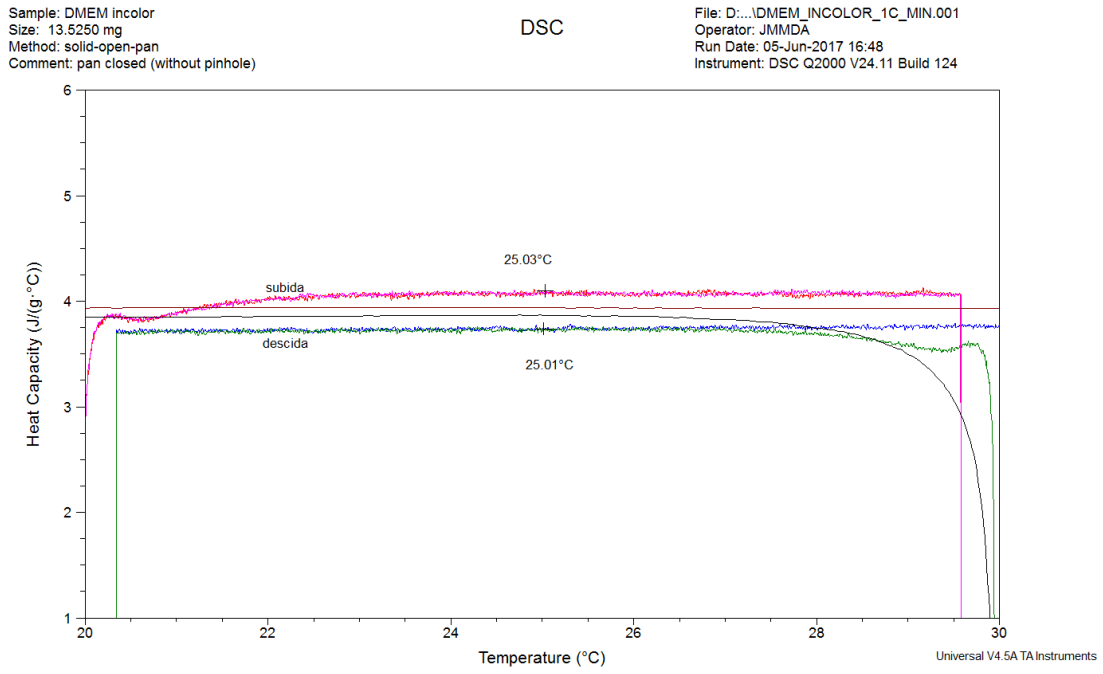

Figure 52: (A) Graphic of heat flow as a function of temperature in DMEM (without phenol red). By doing the punctual tangent in the selected area, a graphic of specific heat as a function of temperature is obtained (B).

Appendix D

Calculating the photothermal yield

The photothermal yield is given by the following formula (**Equation 7**):

$$\eta(\%) = \frac{heat\ transfer(Q)}{absorbed\ energy\ (E)} \times 100 \qquad \textbf{Equation 7}$$

The numerator and the denominator of the fraction have to be quantified separately. Starting with the simple part, the numerator, *heat transfer* is calculated by using **equation 4**.

As for the *absorbed energy*, the following steps need to be taken:

$$I = I0.(1 - 10^{-\overline{Abs}}) \qquad \textbf{Equation 8}$$

- Using **Equation 8**, as starting point, it is a Lambert-Beer law derivation, where I is the light intensity after it passes through the sample, I0 is the initial light intensity and $\overline{Abs}$ is the average between the absorbance before and after the assay. The value of initial light intensity was provided by Pedro Pedrosa, from Actinometry data that was optimized by him according to the conditions used in the calorimetry assay;
- Calculating ***I***, a value of moles of photons per second is obtained;
- Multiplying this value by the **time** of each assay (**180 seconds**), now we have a value in moles of photons;
- Multiplying by Avogadro's number (**6.022E23 mol^{-1}**), obtaining a value in number of photons;
- Using Planck's equation (Δ**E = h.υ**, where E is energy, h is the Planck's constant and has a value of **6.62607004E-34 m^2.kg.s^{-1}**, and υ is the frequency), it is possible to calculate the energy of each photon at a specific wavelength (in this case 532 nm) in Joules;
- If the value of the energy of a photon is known, as well as the number of photons, the energy absorbed by each sample is calculated.

Appendix E

RMN protocol

This protocol was done with the help of the articles of Smith et al, Santoshi et al., and Eugenio Alvarado [65-67].

Phase 1 (Preparing the gold nanoparticles): filter the gold nanoparticles with a citrate capping and then concentrate them through centrifugation at a speed of 14000g. The process is done till 3 mL of filtered AuNPs are converted to 1 mL. Then, proceed with functionalization with different concentrations of the ligand (PEG, with thiolated end), from 0.28 nM to 2.8 nM (use protocol in **subsection 2.4.1** without the part of Ellman's Assay).

The "PEGylated" AuNPs are then concentrated and submitted to digestion with 1 drop (approximately 5 μL) of concentrated aqua regia. The digestion is done overnight before dilution to a total volume of 600 μL (10% D2O to do the lock).

Phase 2 (Data acquisition): use a Bruker 600 Ultrashield magnet with an AVANCE III Console at a 298 K. The following parameters are important in order to achieve great accuracy:

- Do a careful shimming to the sample (this is crucial in order to avoid problems with signal overlapping, so that deconvolution can be done);
- Choose a spectral window so that all peaks of interest fall within 60% of its center. Thus, it will compensate for the signal attenuation that occurs at the spectral edges due to the receiver filters;
- Use solvent suppression (if not deuterated solvent);
- All experiments need a minimum recycle delay of 5 s was used, which is sufficiently greater than T1;
- Use an integration standard (e.g. Acetonitrile).
- Gather enough scans to get a good signal to noise ratio (minimum signal-to-noise ratio of 360).

To do quantitative analysis, the ligand peak was integrated and similarly divided by the known integrated of the reference peak (e.g. Acetonitrile) to calculate the

concentration upon comparison with the calibration curve (previously done). The following figure exemplifies a ^{1}H NMR spectrum of PEG (with thiolated end) in deuterated solvent.

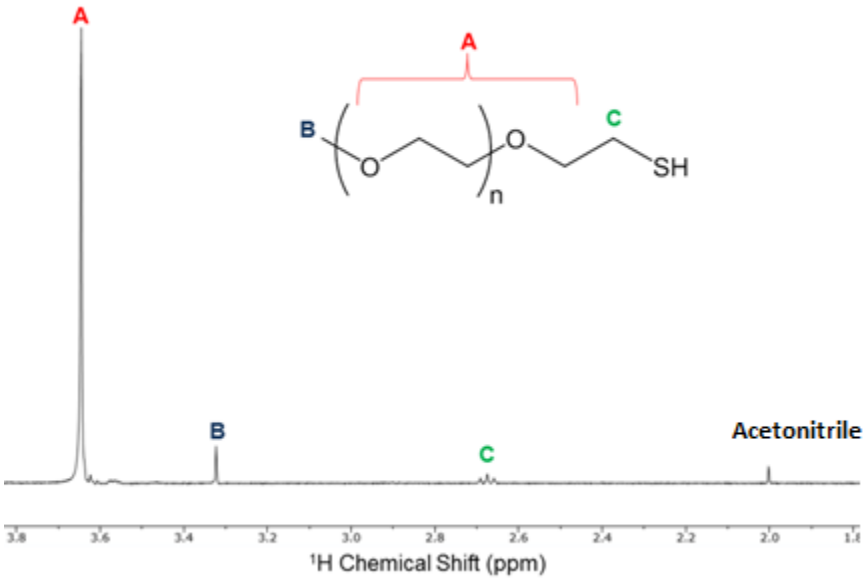

Figure 53: Representative ^{1}H NMR spectrum of PEG (with a thiol end) in deuterated solvent with its labeled structure corresponding to plotted ^{1}H NMR peak locations. [65]

APPENDIX F

Publication

diagnostics

MDPI

Review

Gold Nanoparticles for Diagnostics: Advances towards Points of Care

Mílton Cordeiro [1,2], Fábio Ferreira Carlos [1], Pedro Pedrosa [1], António Lopez [1] and Pedro Viana Baptista [1,*]

[1] UCIBIO, Departamento de Ciências da Vida, Faculdade de Ciências e Tecnologia, Universidade Nova de Lisboa, Campus da Caparica, 2829-516 Caparica, Portugal; m.cordeiro@campus.fct.unl.pt (M.C.); fa.carlos@campus.fct.unl.pt (F.F.C.); pm.pedrosa@campus.fct.unl.pt (P.P.); a.lopez@campus.fct.unl.pt (A.L.)

[2] Rede de Química e Tecnologia (REQUIMTE), Departamento de Química, Faculdade de Ciências e Tecnologia, Universidade Nova de Lisboa, Campus da Caparica, 2829-516 Caparica, Portugal

* Correspondence: pmvb@fct.unl.pt; Tel.: +351-21-294-8530

Academic Editor: Paul Drain
Received: 25 October 2016; Accepted: 18 November 2016; Published: 22 November 2016

Abstract: The remarkable physicochemical properties of gold nanoparticles (AuNPs) have prompted developments in the exploration of biomolecular interactions with AuNP-containing systems, in particular for biomedical applications in diagnostics. These systems show great promise in improving sensitivity, ease of operation and portability. Despite this endeavor, most platforms have yet to reach maturity and make their way into clinics or points of care (POC). Here, we present an overview of emerging and available molecular diagnostics using AuNPs for biomedical sensing that are currently being translated to the clinical setting.

Keywords: gold nanoparticles; diagnosis; point-of-need; biomolecular sensing

1. Introduction

Precise and accurate diagnosis of human related diseases (i.e., genetic disorders, pathogen infection, etc.) is of paramount importance for health care in both developed and developing countries. It ensures that patients have access to the most favorable therapeutic agents in the shortest time span, leading to better prognosis. This translates to significant reductions in the financial burden for health care systems [1]. In developed countries, diagnostics is usually performed at centralized laboratories by specialized personnel. In developing countries, where these infrastructures usually lack the appropriate equipment and/or personnel, accurate diagnosis may be cost-prohibitive and therefore inaccessible [2]. To overcome these bottlenecks, technologies that allow diagnosis at the site of care—point-of-care testing (POCT)—are of extreme importance, allowing for a reduction in sample transportation and processing, use at the point of need, and more importantly, a shorter time between diagnosis and appropriate therapeutic intervention.

The World Health Organization set criteria for POCT, summarized in the acronym "ASSURED"—affordable, sensitive, specific, user-friendly, rapid/robust, equipment-free or minimal and deliverable to those with the greatest need. By fulfilling most of these requirements, POCT should bring not only traditional centralized laboratory-based testing (sensitive and specific) closer to both patients and doctors (user-friendly), but also be suitable for low-income countries where the lack of healthcare facilities is a reality. POCT devices may be grouped into two categories: (i) miniaturized devices with automate sample preparation, analysis and detection to be used on a hand-held basis and (ii) robust devices that allow increased sensitivity for a wide spectrum of analytes to be used at the benchtop [3,4]. The biggest challenge is to make these tests and/or devices consumable and available at a low-cost with reliable results.